

Intervalence (Charge-Resonance) Transitions in Organic Mixed-Valence Systems. Through-Space versus Through-Bond Electron Transfer between Bridged Aromatic (Redox) Centers

D.-L. Sun, S. V. Rosokha, S. V. Lindeman, and J. K. Kochi*

Contribution from the Department of Chemistry, University of Houston, Houston, Texas 77204-5003

Received August 11, 2003; E-mail: jkochi@uh.edu

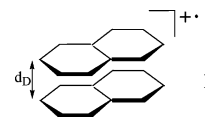
Abstract: Intervalence absorption bands appearing in the diagnostic near-IR region are consistently observed in the electronic spectra of mixed-valence systems containing a pair of aromatic redox centers (Ar^+/Ar) that are connected by two basically different types of molecular bridges. The *through-space* pathway for intramolecular electron transfer is dictated by an *o*-xylylene bridge in the mixed-valence cation radical $\mathbf{3}^{+\bullet}$ with $\text{Ar} = 2,5\text{-dimethoxy-}p\text{-tolyl (T)}$, in which conformational mobility allows the proximal syn disposition of planar T^+/T redox centers. Four independent experimental probes indicate the large through-space electronic interaction between such cofacial Ar^+/Ar redox centers from the measurements of (a) sizable potential splitting in the cyclic voltammogram, (b) quinonoidal distortion of T^+/T centers by X-ray crystallography, (c) “doubling” of the ESR hyperfine splittings, and (d) a pronounced intervalence charge-resonance band. The *through (br)-bond* pathway for intramolecular electron transfer is enforced in the mixed-valence cation radical $\mathbf{2a}^{+\bullet}$ by the *p*-phenylene bridge which provides the structurally inflexible and linear connection between Ar^+/Ar redox centers. The direct comparison of intramolecular rates of electron transfer (k_{ET}) between identical T^+/T centers in $\mathbf{3}^{+\bullet}$ and $\mathbf{2a}^{+\bullet}$ indicates that *through-space* and *through-bond* mechanisms are equally effective, despite widely different separations between their redox centers. The same picture obtains for $\mathbf{3}^{+\bullet}$ and $\mathbf{2a}^{+\bullet}$ from theoretical computations of the first-order rate constants for intramolecular electron transfer from Marcus–Hush theory using the electronic coupling elements evaluated from the diagnostic intervalence (charge-transfer) transitions. Such a strong coherence between theory and experiment also applies to the mixed-valence cation radical $\mathbf{7}^{+\bullet}$, in which the aromatic redox **S** center is sterically encumbered by annulation.

Introduction

Singer, Fraenkel, and co-workers¹ were among the first to discover the interesting (intermolecular) association of aromatic cation radicals ($\text{ArH}^{+\bullet}$) with their parent π -donors (ArH) via the observation of “doubled” ESR spectra in naphthalene and related hydrocarbons.² Soon thereafter, Badger, Brocklehurst, et al.³ observed the characteristic UV–vis absorptions of *dimer cation radicals* $(\text{ArH})_2^{+\bullet}$ by γ -radiolysis of frozen naphthalene and other arene solutions in alkane matrix; they proposed the diagnostic (near-IR) bands to be derived via “charge-resonance” transitions from electron delocalized ground states comprised of cofacial ArH^+/ArH pairings.⁴ However, it was not until later that single-crystal X-ray crystallographic analysis⁵ confirmed

this speculative structure for the cationic naphthalene dimer **1** (Chart 1), in which the parallel pair of equivalent arene moieties is separated by the very long (noncovalent) distance of $d_{\text{D}} = 3.20 \text{ \AA}$ but yet is significantly closer than the (nonbonded) van der Waals sum of $d_{\text{vdW}} = 3.50 \text{ \AA}$.

Chart 1



In a much more general context, a positively charged (paramagnetic) binary unit such as **1** is integral to a wide array

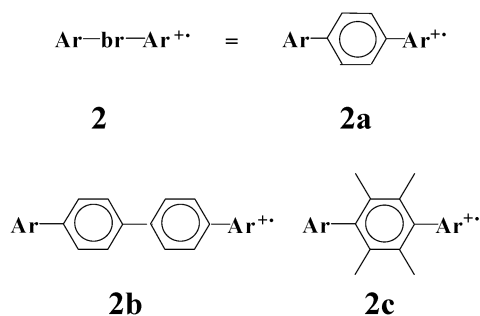
- (1) (a) Lewis, I. C.; Singer, I. C. *Chem. Phys.* **1965**, *43*, 2712. (b) Howarth, O. W.; Fraenkel, G. K. *J. Am. Chem. Soc.* **1966**, *88*, 4514. (c) Howarth, O. W.; Fraenkel, G. K. *J. Chem. Phys.* **1970**, *52*, 6258.
 (2) (a) Gerson, F.; Kaupp, G.; Ohya-Nishiguchi, H. *Angew. Chem., Int. Ed.* **1977**, *16*, 657. (b) Wartin, A. R.; Valenzuela, J.; Staab, H. A.; Neugebauer, F. A. *Eur. J. Org. Chem.* **1998**, *139*, 9. (c) Lau, W.; Kochi, J. K. *J. Org. Chem.* **1986**, *51*, 1801.
 (3) (a) Badger, B.; Brocklehurst, B.; Russell, R. D. *Chem. Phys. Lett.* **1967**, *1*, 122. (b) Badger, B.; Brocklehurst, B. *Nature* **1968**, *219*, 263. (c) Badger, B.; Brocklehurst, B. *Trans. Faraday Soc.* **1969**, *65*, 2582. (d) Badger, B.; Brocklehurst, B. *Trans. Faraday Soc.* **1969**, *65*, 2588. (e) Badger, B.; Brocklehurst, B. *Trans. Faraday Soc.* **1970**, *66*, 2939.

- (4) See also: (a) Meot-Ner, M.; Hamlet, P.; Hunter, E. P.; Field, F. H. *J. Am. Chem. Soc.* **1978**, *100*, 5466. (b) Meot-Ner, M. *J. Phys. Chem.* **1980**, *84*, 2724. (c) Meot-Ner, M.; El-Shall, M. S. *J. Am. Chem. Soc.* **1986**, *108*, 4386. (d) Masnovi, J. M.; Kochi, J. K. *J. Phys. Chem.* **1987**, *91*, 1878. (e) Kochi, J. K.; Rathore, R.; Le Magueres, P. *J. Org. Chem.* **2000**, *65*, 6826. (f) Note that dimer cation radicals such as **1** belong to a larger, more diverse group of paramagnetic (complex) associates comprised of π -radicals and their neutral precursors such as anion radical/electron acceptor, π -radical/ π -cation, etc. for which the general term “pimer” has been recently proposed. (g) See: Ganesan, V.; Rosokha, S. V.; Kochi, J. K. *J. Am. Chem. Soc.* **2003**, *125*, 2559. Lu, J.-M.; Rosokha, S. V.; Kochi, J. K. *J. Am. Chem. Soc.* **2003**, *125*, 12161.

of stacked arene structures in the crystalline solid state, in which intermolecular communication relies on hole (electron) hopping—as in molecular metals (wires), optoelectronic devices, electrical conductors, magnets, etc. of potential development for organic material science.^{7,8} To this end, we now inquire as to the more basic evaluation of those structural factors leading to the charge-resonance transitions inherent to dimer cation radicals such as **1**. Owing to the experimental difficulty of “isolating” **1** as a separate unit in a stacked (crystalline) lattice, it is desirable to develop discrete molecular systems for the quantitative study in solution of how electron (hole) transfer can occur within ArH⁺/ArH dyads.

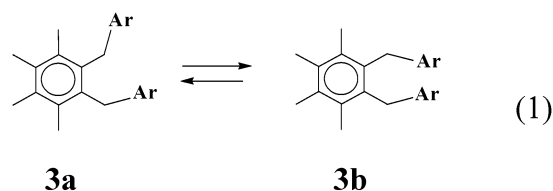
In earlier studies,⁹ we discussed the organic mixed-valence system **2**, as shown in Chart 2, in which various (poly)*p*-phenylene structures ensure structural rigidity and can be utilized

Chart 2

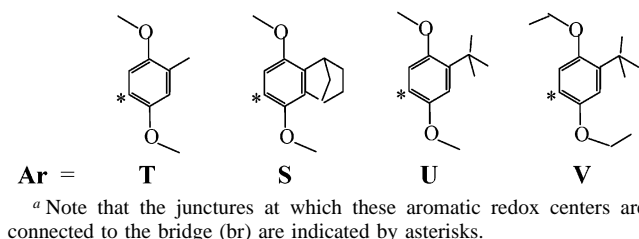


as molecular bridges (br) in the study of intramolecular electron transfer between the Ar⁺/Ar redox centers, primarily *through (br) bond* in the superexchange (hole-hopping) mechanism.^{9b,10–12} In this study, we examine the conformationally flexible system **3**, in which the preponderance of the highly mobile equilibrium (i.e. Chart 3) leads to the juxtaposition of a pair of Ar groups in conformer **3b**. The resulting cofacial orientation of the two aromatic planes is reminiscent of that in the intermolecular dimer cation radical **1**; **3b** thus represents the prototypical donor to examine the direct *through-space* interaction of Ar⁺/Ar (redox) centers in organic mixed-valence systems. For quantitative studies of the energetics, structures, and optical transitions in

Chart 3



such dimer cation-radical assemblies, we focus on Ar = 2,5-dimethoxy-*p*-tolyl (**T**), owing to the reversible oxidation of this aromatic group to generate its persistent cation radical (**T**⁺) at an accessible potential of $E^{\circ}_{\text{ox}} = 1.10 \text{ V vs SCE}$.^{13–15}

Chart 4^a

Results

I. Synthesis and Conformational Structure of Mixed-Valence Donors. A. Synthesis.

The series of mixed-valence donors **3–5** as identified in Table 1 are governed by the distinctive aromatic redox center **T** in Chart 4. The attachment of **T** to the *o*-xylylene bridge in **3** was effected by treatment of 1,2-bis(bromomethyl)tetramethylbenzene with stoichiometric

Table 1. Structures and Oxidation Potentials of Mixed-Valence Donors and Their Mononuclear Models^a

Mixed-Valence Donor	$E_{1/2}$ (V vs SCE) ^{ab}	Mixed-Valence Donor	$E_{1/2}$ (V vs SCE) ^{ab}
3	1.07 (1e) 1.23 (1e)	7	1.14 (2e)
4	1.13 (2e)	8 CH_3-S	1.14
5	1.13 (2e)	9	1.06 (1e) 1.14 (1e)
6 CH_3-T	1.10 (1e)	10	1.06 (1e) 1.15 (1e)

^a For structural identification of the redox center **T**, etc., see Charts 4 and 5. ^b Reversible cyclic voltammograms measured at $v = 2 \text{ V s}^{-1}$. In parentheses are given the number of electrons transferred.

- (5) (a) Fritz, H. P.; Gebauer, H.; Friedrich, P.; Ecker, P.; Artes, R.; Schubert, V. Z. *Naturforsch.* **1978**, *33B*, 498. (b) Fritz, H. P.; Gebauer, H.; Friedrich, F.; Schubert, V. *Angew. Chem.* **1978**, *90*, 305. (c) Enkelmann, V.; Morra, B. S.; Kröhnke, C.; Wegner, G. *Chem. Phys.* **1982**, *66*, 303. (d) Enkelmann, V. *Adv. Chem. Ser.* **1988**, *No. 217*, 177. (e) Herwig, P. T.; Enkelmann, V.; Schmelz, D.; Müllen, K. *Chem. Eur. J.* **2000**, *6*, 1834.
- (6) See also: (a) Keller, H. J.; Nöthe, D.; Pritzkow, H.; Wehe, D.; Werner, M. *Mol. Cryst.* **1980**, *62*, 181. (b) Endres, H.; Keller, H.; Müller, B.; Schweitzer, D. *Acta Crystallogr.* **1985**, *C41*, 607. (c) Stenger-Smith, J. D.; Lenz, R. W.; Enkelmann, V.; Wegner, G. *Makromol. Chem.* **1992**, *193*, 515. (d) Note that Chart 1 is only intended to emphasize pictorially the parallel sandwich arrangement of the two naphthalene moieties, which are actually rotated in the plane by 90° relative to each other.
- (7) (a) Miller, J. S. *Inorg. Chem.* **2000**, *39*, 4392. (b) Williams, J. M. *Organic Superconductors (Including Fullerenes): Synthesis, Structure, Properties and Theory*; Prentice Hall: Englewood Cliffs, NJ, 1992. (c) Ferraro, J. R.; Williams, J. M. *Introduction to Synthetic Electrical Conductors*; Academic Press: Orlando, FL, 1987. (d) Farges, J.-P., Ed. *Organic Conductors: Fundamentals and Applications*; Marcel Dekker: New York, 1994.
- (8) (a) Lahti, P. M., Ed. *Magnetic Properties of Organic Materials*; Marcel Dekker: New York, 1999. (b) Miller, J. S.; Drillon, M., Eds. *Magnetism: Molecules to Materials*; Wiley-VCH: Weinheim, Germany, 2001.
- (9) (a) Lindeman, S. V.; Rosokha, S. V.; Sun, D.-L.; Kochi, J. K. *J. Am. Chem. Soc.* **2002**, *124*, 843. (b) Rosokha, S. V.; Sun, D.-L.; Kochi, J. K. *J. Phys. Chem. A* **2002**, *106*, 2283. (c) Sun, D.-L.; Lindeman, S. V.; Rathore, R.; Kochi, J. K. *J. Chem. Soc., Perkin Trans. 2* **2001**, 1585. (d) Note that the direct observation of the (Ar-to-br) charge-transfer absorption bands in the mixed-valence complexes **2**^{9b} allowed the superexchange mechanism to be quantitatively evaluated by the Creutz, Newton, Sutin (CNS) methodology.¹⁰

- (10) Creutz, C.; Newton, M. D.; Sutin, N. *J. Photochem. Photobiol. A: Chem.* **1994**, *82*, 47.
- (11) For previous use of organic mixed-valence systems for intramolecular electron-transfer studies, see: (a) Nelsen, S. F.; Adamus, J.; Wolff, J. J. *J. Am. Chem. Soc.* **1994**, *116*, 1589. (b) Nelsen, S. F.; Trieber, D. A.; Wolff, J. J.; Powell, D. R.; Rogers-Crowley, S. *J. Am. Chem. Soc.* **1997**, *119*, 6873. (c) Lambert, C.; Noll, G. *J. Am. Chem. Soc.* **1999**, *121*, 8434. (d) Holzapfel, M.; Lambert, C.; Selinka, C.; Stalke, D. *J. Chem. Soc., Perkin Trans. 2* **2002**, 1553.
- (12) See also: (a) Rak, S. F.; Miller, L. L. *J. Am. Chem. Soc.* **1992**, *114*, 1388. (b) Lahlil, K.; Moradpour, A.; Bowlas, C.; Menou, F.; Cassoux, P.; Bonvoisin, J.; Launay, J.-P.; Dive, G.; Dehareng, D. *J. Am. Chem. Soc.* **1995**, *117*, 9995. (c) Nelsen, S. F.; Ramm, M. T.; Wolff, J. J.; Powell, D. R. *J. Am. Chem. Soc.* **1997**, *119*, 6863. (d) Nelsen, S. F.; Ismagilov, R. F.; Powell, D. R. *J. Am. Chem. Soc.* **1997**, *119*, 10213. (e) Gautier, N.; Dumur, F.; Lloveras, Vidal-Gancedo, J.; Veciana, J.; Rovira, C.; Hudhomme, P. *Angew. Chem., Int. Ed.* **2003**, *42*, 2765.
- (13) Rathore, R.; Kumar, A. S.; Lindeman, S. V.; Kochi, J. K. *J. Org. Chem.* **1998**, *63*, 5847.
- (14) Ebersson, L. *Electron-Transfer Reactions in Organic Chemistry*; Springer-Verlag: New York, 1987.

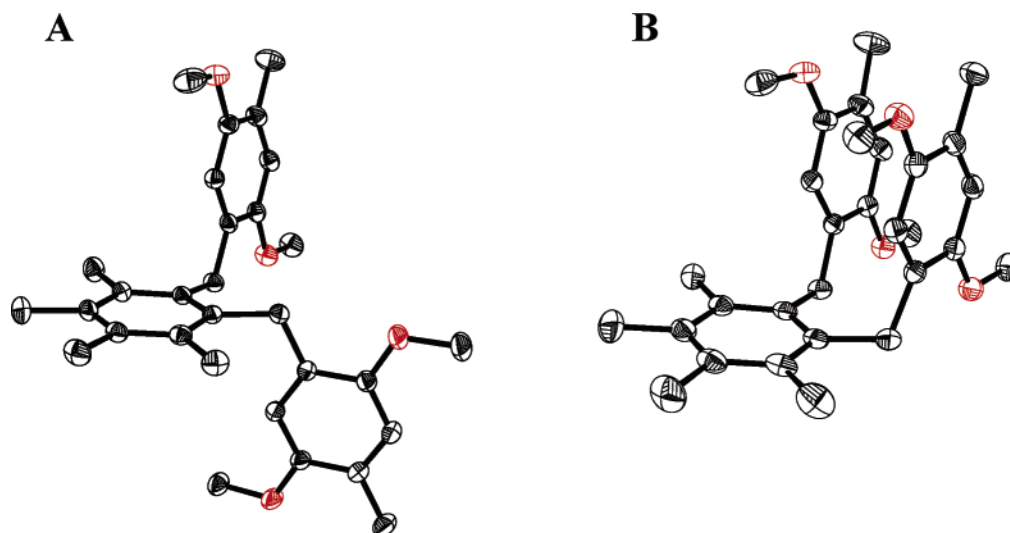


Figure 1. ORTEP diagrams of the *o*-xylylene-bridged mixed-valence donor **3** and its cation radical **3**^{•+} (as the SbCl₆[−] salt) showing the two **T** centers with anti conformation in the neutral donor (A) and syn conformation in the cation radical (B). Note that all hydrogens are omitted for clarity.

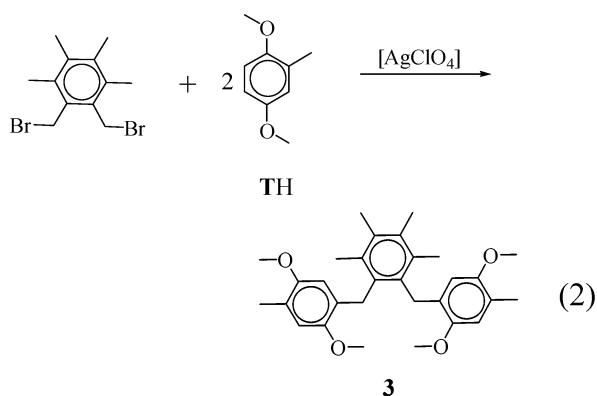
Table 2. X-ray Structural Parameters of the Redox Centers in the Mixed-Valence Donors and Their Cation Radicals^a

T =

	[σ] ^b		$\alpha\alpha'$	$\beta\beta'$	$\gamma\gamma'$	$\delta\delta'$	$\epsilon\epsilon'$	q^c
3	0.003	T ^d	1.400/1.399 [1.400]	1.397/1.396 [1.397]	1.397/1.398 [1.398]	1.376/1.377 [1.377]	1.424/1.426 [1.425]	0
3 ^{•+} PF ₆ [−]	0.002	T ^d	1.417/1.416 [1.417]	1.402/1.399 [1.401]	1.380/1.387 [1.384]	1.347/1.349 [1.348]	1.434/1.436 [1.435]	+0.5
3 ^{•+} SbCl ₆ [−]	0.004	T ¹	1.430/1.431 [1.431]	1.406/1.398 [1.402]	1.362/1.363 [1.363]	1.327/1.328 [1.428]	1.440/1.436 [1.438]	+0.9
		T ²	1.396/1.400 [1.398]	1.396/1.390 [1.393]	1.371/1.380 [1.376]	1.368/1.365 [1.367]	1.433/1.425 [1.429]	+0.1
T ^{•+} (CH ₂) ₃ T ^{•+} ^e	0.004	T ^d	1.447/1.447 [1.447]	1.407/1.408 [1.407]	1.369/1.375 [1.372]	1.324/1.329 [1.327]	1.457/1.457 [1.457]	+1.0

^a Average bond lengths (Å) in brackets. ^b Average experimental precision. ^c Estimate of positive charge parameter evaluated as described in the text. ^d Parameters for both donor groups are identical. ^e Data from ref 9a, for comparison.

amounts of **TH** and silver(I) perchlorate¹⁶



and the isomeric bridged donors **4** and **5** were prepared by an analogous procedure from the *m*- and *p*-dibromo precursors.¹⁷

(15) (a) Analogous studies have also been carried out with the phenothiazinyl (**P**) redox center, in which the larger intrinsic barrier ($\lambda/4$) for electron transfer of approximately 7–8 kcal mol^{−1} relative to the corresponding barrier of the dimethoxytolyl redox center of ~5 kcal mol^{−1} arises from the significant configurational change of the tub-shaped donor center **P** to its planar cation radical **P**^{•+} upon electron transfer. (b) Sun, D.-L.; Rosokha, S. V.; Kochi, J. K. *J. Am. Chem. Soc.*, in press.

To modulate the steric hindrance at the planar redox center, it was modified by bicyclic annulation as in redox center **S** and by *tert*-butyl substitution as in redox centers **U** and **V** (Chart 4); the corresponding mixed-valence donors **7**, **9**, and **10** were synthesized by essentially the same procedure (see the Experimental Section).

B. Conformational Structure. Single colorless crystals of the ortho-bridged mixed-valence donor **3**, isolated by the controlled slow removal of solvent, consisted of the stable anti conformation **3a** in eq 1, as shown by the ORTEP diagram in Figure 1A. Otherwise, both **T** centers in **3** have the usual planar centrosymmetric benzenoid geometry, as evaluated by the bond lengths and angles—the endocyclic α , β , and γ as well as the exocyclic δ and ϵ bonds being within the standard range (Table 2). For the accompanying spectral/computational examination of the dynamic equilibrium in eq 1, see details in the Experimental Section.

II. Electrochemical Generation of Mixed-Valence Systems. Selective oxidations of the aromatic donors in Table 1 to the relevant mixed-valence cation radicals were first examined by

(16) Závada, J.; Pánková, M.; Aenold, Z. *Collect. Czech. Chem. Commun.* **1976**, *41*, 1777.

(17) Závada, J.; Pánková, M.; Holý, P.; Tichý, M. *Synthesis* **1994**, *11*, 1132.

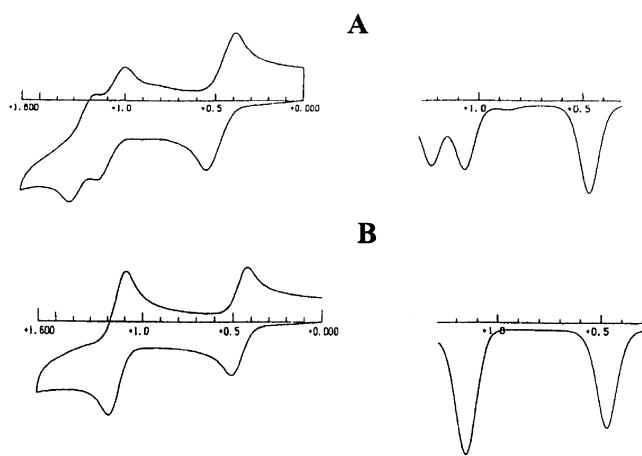
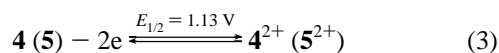


Figure 2. Initial positive-scan cyclic voltammogram (left) and Osteryoung square wave voltammogram (right) of the ortho-bridged mixed-valence donor **3** (A) and meta-bridged isomer **4** (B), including the ferrocene internal standard at 0.5 V. (Note that the electrochemical behavior of the para-bridged mixed-valence donor **5** coincides with that of **4**).

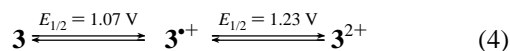
transient electrochemical techniques in 1 mM dichloromethane solution containing 0.2 M tetra-*n*-butylammonium hexachlorophosphate as supporting electrolyte. Two distinctive anodic behaviors were observed with the isomeric bridged donors **3–5** in the initial positive-scan cyclic voltammograms obtained with a platinum electrode at a standard scan rate of $\nu = 2 \text{ V s}^{-1}$.

(A) With the *m*-xylylene- and *p*-xylylene-bridged isomers **4** and **5**, the reversible cyclic voltammograms (Figure 2B) showed a single two-electron anodic wave (corresponding to two unresolved one-electron processes) at a potential of $E_{1/2} = 1.13 \text{ V}$ vs SCE:



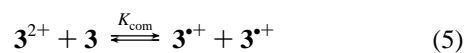
This oxidation potential coincided with the reversible one-electron oxidation of donor **6**, which represented the mono-nuclear model for the unambiguous oxidation of a lone **T** center to the full cation radical **T^{•+}** (compare entries for **4–6** in Table 1).

(B) In contrast, the reversible cyclic voltammogram of the isomeric *o*-xylylene-bridged donor **3** consisted of a pair of oxidation waves at $E_{1/2} = 1.07$ and 1.23 V, with each wave corresponding to a one-electron process in Figure 2A, so that the initial production of the mixed-valence cation radical was separately followed by its subsequent oxidation to the dication:



The unique cyclic voltammetric behavior of the ortho-bridged isomer **3** indicated that the initial oxidation of a **T** center to its cation radical **T^{•+}** was different from that of the second aromatic center, whereas in the meta and para isomers, the two **T** centers were both oxidized at identical potentials. (It follows that the dication in eq 4 actually consisted of a pair of equivalent, but separate, cation-radical centers, as was later established from its ESR spectrum (vide infra).) As such, the difference between the first and second potentials, $\Delta E = E_{1/2}(2) - E_{1/2}(1)$, reflected

the energetics of the dication comproportionation:¹⁸



and the position of the equilibrium was quantitatively evaluated from the splitting: $\Delta E = -\Delta G_{\text{com}}/F$, where F is the Faraday constant and ΔG_{com} is the Gibbs free-energy change. Most importantly, the major component of the cation-radical stabilization, i.e., $-RT \ln K_{\text{com}}$, is the electronic interaction between the pair of **T/T^{•+}** redox centers.¹⁹ Thus, the stabilization energy of the ortho-bridged cation radical **3^{•+}** was evaluated as 2 kcal/mol, whereas $\Delta G_{\text{com}} = 0$ for the meta and para isomers. To analyze such mixed-valence cation radicals, we now focus primarily on the isolation and X-ray crystallographic analysis of the bridged structures together with the spectral analysis (UV–vis–near-IR) of their diagnostic charge-resonance absorption bands and the characteristics of the temperature-dependent line broadenings in the ESR spectra as follows.

III. Isolation and X-ray Crystallography of Mixed-Valence Cation Radicals. Controlled-potential oxidation of the *o*-xylylene-bridged donor **3** at the foot of the first anodic CV wave (1.00 V, Figure 2a) afforded a quantitative yield of the mixed-valence cation radical **3^{•+}**, but complete separation of the pure salt from the supporting electrolyte proved difficult. Accordingly, we employed the quantitative chemical oxidation with a series of bona fide one-electron oxidants, including nitrosonium (**NO⁺**) salts,²⁰ antimony pentachloride,²¹ and various organic cation radicals of octamethylnaphthalene²² and tris(dibromophenyl)amine.²³ Indeed, all of these reagents afforded excellent yields of crystalline **3^{•+}** salts, but the particularly easy removal of the gaseous reduction product of **NO⁺** facilitated the isolation of bright yellow single crystals of **3^{•+}**SbCl₆[−] and **3^{•+}**PF₆[−] for X-ray crystallographic analysis.

The prominent feature of the ORTEP diagram of the mixed-valence cation radical **3^{•+}** in Figure 1B is the mutually syn conformation of the two planar **T** centers—with the nearly parallel rings offset by a dihedral angle of only 10°. Such a cofacial arrangement occurs with the interplanar separation of $d_D = 3.2 \text{ \AA}$, which is the same as that in dimer cation radicals such as **1** (see Chart 1) and roughly 10% shorter than the van der Waals contact. The latter pointed to significant electronic interaction of the two **T** redox centers in **3^{•+}**, which was further confirmed by close scrutiny of the X-ray bonding parameters in the following way. First, the removal of a full electron from a lone (noninteracting) **T** center is accompanied by a diagnostic quinonoid distortion, which derives from the selective elongation of the α and β bonds and concomitant contraction of the γ and δ bonds in **T^{•+}**, as compared in the first and last entries of Table 2. Second, the quantitative relationship between quinonoid distortion and removal of (partial) charge q_i from a **T** center is then given by $q_i = (d_0 - d_i)/(d_0 - d_1)$,²⁴ where d_0 and d_1 are

- (18) (a) Creutz, C. *Prog. Inorg. Chem.* **1983**, *30*, 1. (d) Demadis, K. D.; Hartshorn, C. M.; Meyer, T. *J. Chem. Rev.* **2001**, *101*, 2655.
 (19) (a) Astruc, D. *Electron Transfer and Radical Processes in Transition-Metal Chemistry*; VCH: New York, 1995. (b) Evans, C. E. B.; Naklicki, M. L.; Rezvani, A. R.; White, C. A.; Kondratiev, V. V.; Crutchley, R. J. *J. Am. Chem. Soc.* **1998**, *120*, 13096.
 (20) Lee, K. Y.; Kuchynka, D. J.; Kochi, J. K. *Inorg. Chem.* **1990**, *29*, 4196.
 (21) (a) Bell, F. A.; Ledwith, A.; Sherrington, D. C. *J. Chem. Soc. C* **1969**, *13*, 2719. (b) Luken, E. A. C. *J. Chem. Soc.* **1969**, 4963.
 (22) Rosokha, S. V.; Kochi, J. K. *J. Am. Chem. Soc.* **2001**, *123*, 8985.
 (23) Schmidt, W.; Steckman, E. *Chem. Ber.* **1980**, *113*, 577.
 (24) Le Magueres, P.; Lindeman, S. V.; Kochi, J. K. *J. Chem. Soc., Perkin Trans. 2* **2001**, 1180.

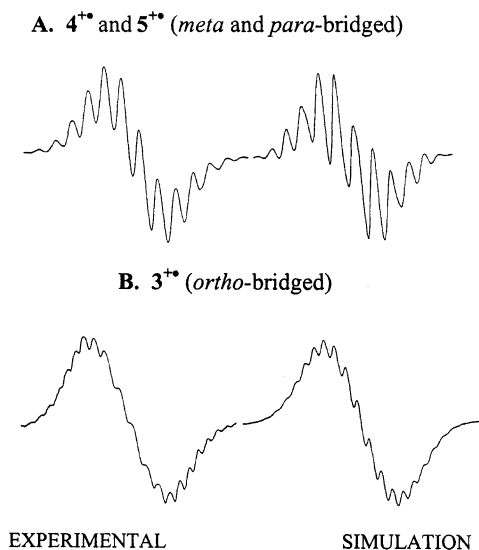


Figure 3. Comparison of the experimental (left) and computer-simulated (right) ESR spectra of mixed-valence cation radicals of the meta-/para-bridged $4^{+\bullet}/5^{+\bullet}$ (A) with that of the ortho-bridged isomer $3^{+\bullet}$ showing doubled hyperfine splittings (B) in dichloromethane solution.

the bond lengths in the neutral **T** and the cation radical $\mathbf{T}^{+\bullet}$, respectively, and d_i is the bond length in the relevant **T** center of the mixed-valence cation radical ($3^{+\bullet}$). For clarity, we selected the δ bonds for calculation of q_i owing to their having the largest (bond-length) change upon oxidation; these values are listed in the last column of Table 2. Third and most striking is the value of $q_i = +0.5$ for $3^{+\bullet}\text{PF}_6^-$ (second entry in Table 2) reflecting the equal distribution of positive charge between *both* redox centers. Accordingly, the structure of each **T** center in $3^{+\bullet}$ is precisely intermediate between those of **T** and $\mathbf{T}^{+\bullet}$ to reflect complete odd-electron delocalization between two equivalent redox centers.²⁵ Fourth, the charge distribution in $3^{+\bullet}$ is counterion dependent, with $q_i = +0.9$ on one **T** center (and $+0.1$ on the other) in the hexachloroantimonate salt (third entry). As such, the asymmetric charge distribution in $3^{+\bullet}\text{SbCl}_6^-$ reflects only limited (electron) delocalization extant between these redox centers in this crystalline salt, and the charge is essentially localized on one **T** center, while the other remains (nearly) neutral.

IV. ESR Spectra and Their Line Broadening in Mixed-Valence Cation Radicals. A. Temperature-Independent ESR Spectra. The meta- and para-bridged mixed-valence cation radicals $4^{+\bullet}$ and $5^{+\bullet}$ in dichloromethane solutions afforded the (identical) ESR spectra shown in Figure 3A (left). The spectra bore a strong resemblance to that of the mononuclear model $6^{+\bullet}$, in which the hyperfine coupling constants for three sets of equivalent protons have been established as $a_{\text{CH}_3\text{O}} = 3.12$ G, $a_{\text{CH}_3} = 4.37$ G, and $a_{\text{H}} = 0.48$ G.²⁶ Starting from these values, we optimally simulated the ESR spectrum shown in Figure 3A (right) with the hyperfine coupling constants listed in Table 3 (entries 3 and 4). Most importantly, the ESR spectra of $4^{+\bullet}$ – $6^{+\bullet}$ were all singularly unaffected by temperature changes in the range between 20 and -90 °C.

(25) The absence of crystallographic elements of symmetry in the acentric $\mathbf{T}^{+\bullet}$ center rules out crystal disorder, and the value of $q_i = +0.5$ necessarily reflects the inherent nature of 50/50 charge distribution in $3^{+\bullet}\text{PF}_6^-$. For discussion of this point, see Lindeman et al. in ref 9a.

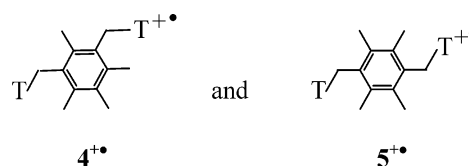
(26) Forbes, W. F.; Sullivan, P. D. *J. Phys. Chem.* **1968**, *48*, 1411.

Table 3. ESR Spectral Parameters of Mixed-Valence Cation Radicals (MVCR) and their Mononuclear Models

MVCR	hyperfine splitting (G) ^a		
	OCH ₃	CH _n	ArH
$3^{+\bullet}$	1.6 (12)	2.3 (6), 3.5 (4)	0.3 (4)
3^{2+}	3.1 (6)	4.6 (3), 6.8 (2)	0.5 (2)
$4^{+\bullet}$	3.2 (6)	4.5 (3), 6.9 (2)	0.5 (2)
4^{2+}	3.1 (6)	4.6 (3), 6.8 (2)	0.5 (2)
$5^{+\bullet}$	3.2 (6)	4.5 (3), 6.9 (2)	0.5 (2)
5^{2+}	3.1 (6)	4.6 (3), 6.8 (2)	0.5 (2)
$6^{+\bullet b}$	3.12 (6)	4.37 (6)	0.48 (2)
$7^{+\bullet}$	3.2 (6)	2.8 (1), 7.0 (2)	0.5 (1)
$8^{+\bullet}$	3.2 (6)	4.0 (4)	0.5 (1)
$9^{+\bullet c}$	1.6 (12)	3.5 (4), 2.3 (6)	0.3 (4)
$10^{+\bullet c}$	1.5 (8)	3.5 (4), 2.3 (6)	0.3 (4)

^a In parentheses are given the number of splitting protons. ^b From ref 26. ^c See the Experimental Section.

The unchanging ESR spectra of $4^{+\bullet}$ and $5^{+\bullet}$ relative to $6^{+\bullet}$ indicated that the paramagnetic redox center in the meta- and para-bridged mixed-valence cation radicals showed no extra temperature-dependent behavior that was not present in the mononuclear cation radical.²⁷ In other words, the unpaired electron in either the *m*-xylylene- and *p*-xylylene-bridged cation radical is frozen on a single $\mathbf{T}^{+\bullet}$ redox center



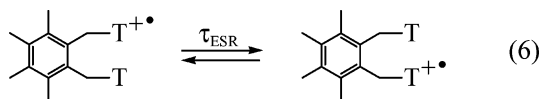
and any dynamic exchange with the other **T** center was too slow to be observed in this temperature range. Moreover, the ESR spectra of the dication 4^{2+} and 5^{2+} were essentially identical (Table 3 and Figure S1 in the Supporting Information) and the hyperfine splittings were the same as those in the mixed-valence cation radicals $4^{+\bullet}$ and $5^{+\bullet}$. The absence of line broadening in the same temperature range indicated each paramagnetic redox center was isolated, and any electromagnetic interaction between these equivalent $\mathbf{T}^{+\bullet}$ centers was too small to be detected in the meta- and para-bridged dication on the ESR time scale.²⁸

B. Temperature-Independent but “Doubled” ESR Spectrum. The ESR spectrum of the ortho-bridged mixed-valence cation radical $3^{+\bullet}$ in Figure 3B (left) showed many more hyperfine lines than that of either the meta ($4^{+\bullet}$) or para ($5^{+\bullet}$) isomers in Figure 3A. Most notably, the computer simulation shown in Figure 3B (right) was derived from twice the number of protons in each of the four sets of equivalent protons with approximately half the coupling constants (Table 3, first entry) relative to those found in the meta and para isomers (second and third entries). Such increased numbers and decreased

(27) For the accompanying ESR effects of methoxyl rotation, see: Sullivan, P. D. *J. Phys. Chem.* **1970**, *74*, 2563.

(28) (a) Although transient electrochemistry showed that the further oxidation of the mixed-valence cation radical $3^{+\bullet}$ could be carried out reversibly, all attempts to isolate crystalline salts of the 3^{2+} dication suitable for X-ray crystallography were unsuccessful (vide infra), owing to the competing decomposition pathway(s). Nonetheless, 3^{2+} was sufficiently persistent to show that its ESR spectrum (see Figure S1) is essentially identical with those of the meta and para isomers 4^{2+} and 5^{2+} and the mononuclear model $6^{+\bullet}$. (b) The partially unstable or metastable character of 3^{2+} suggests that there is some electronic interaction between a pair of $\mathbf{T}^{+\bullet}$ centers in this dication. For the resonance “stabilization” of such a pair of cofacial cation radicals to cation-radical dimers, see Lu et al. in ref 4g.

splittings of hyperfine lines were characteristic of other dimer cation radicals reported previously²⁹ and indicated that either the unpaired electron in the ortho-bridged $3^{+\bullet}$ is completely delocalized over both redox centers or electron exchange between the redox centers

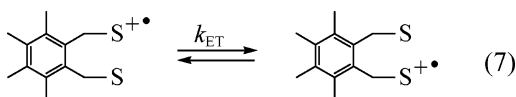


is too fast to be resolved on the ESR time scale with the half-life $\tau_{\text{ESR}} < 10^{-9}$ s. Moreover, the temperature-independent ESR spectra over the 110 °C temperature range relegated the half-life for any dynamic electron exchange to be immeasurably fast even at -90 °C.

C. Line Broadening in ESR Spectra. Mixed-valence donors with encumbered bulky redox-centers were prepared in two forms (Chart 4)—with bicyclic annulation (**S**) and with *tert*-butyl substitutions (**U** and **V**) that were found to be effective in previous studies of sterically hindered associations.³⁰

The ortho-bridged donor **7** with a pair of **S** groups afforded its persistent mixed-valence cation radical much like the ortho-bridged donors **9** and **10** with **U** and **V** centers. However, the ESR spectrum of the sterically hindered $7^{+\bullet}$ at -90 °C bore little resemblance to the delocalized ESR spectrum of the ortho-bridged analogue $3^{+\bullet}$ with $T^{+\bullet}$ centers; it was instead more like that of the localized meta- and para-bridged isomers, $4^{+\bullet}$ and $5^{+\bullet}$. Indeed, this ESR spectrum was strikingly similar to the ESR spectrum of the sterically hindered cation radical $8^{+\bullet}$ of the mononuclear model donor **SCH**₃, and computer simulation with the same hyperfine coupling constants in Table 3 confirmed the spectral assignment.

The ESR spectrum of sterically hindered $7^{+\bullet}$ gradually broadened as the temperature was progressively raised. The uniform broadening of all the lines is shown in Figure 4 (left); and the completely reversible line broadening was attributed to dynamic electron exchange between the pair of redox centers $S^{+\bullet}$ in the ortho-bridged cation radical $7^{+\bullet}$:



Computer simulation of this intramolecular process was carried out with the aid of the ESR-EXN program,³¹ and Figure 4 includes the close fits to the experimental ESR spectra (right) with the first-order rate constants $k_{\text{ET}} = 5 \times 10^6 \text{ s}^{-1}$ at -60 °C and $4 \times 10^7 \text{ s}^{-1}$ at -20 °C. The temperature variation of the rate constants afforded an Arrhenius activation energy of 6.2 kcal/mol and preexponential factor of $10^{12.6} \text{ s}^{-1}$ (Figure S5, Supporting Information). By comparison, the sterically hindered (*tert*-butyl) analogues $9^{+\bullet}$ and $10^{+\bullet}$ both afforded rather complex doubled ESR spectra (see Table 3), but they were not rigorously assigned, since the hyperfine lines showed no signs of broadening in this temperature range.

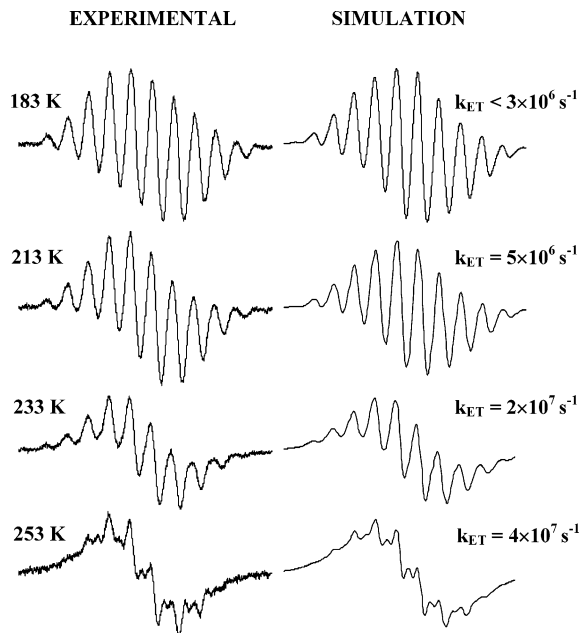


Figure 4. Temperature-dependent ESR line broadening of the mixed-valence cation radical $7^{+\bullet}$ with sterically hindered redox centers $S^{+\bullet}/S$ (left) in comparison with the computer-simulated spectra (right) based on first-order electron exchange.

V. Intervalence (Charge-Resonance) Transition in Mixed-Valence Cation Radicals. The distinguishing feature in the electronic spectra of both *meta* and *para*-bridged mixed-valence cation-radicals $4^{+\bullet}$ and $5^{+\bullet}$ was the well-resolved UV–Vis absorption with $\lambda_{\text{max}} = 438$ and 462 nm (Figure 5A, Table 4) in dichloromethane solution. Since these absorption bands were also the same as those that characterized the mononuclear model $6^{+\bullet}$, they were assigned to the local π – π^* transitions in the $T^{+\bullet}$ redox center. By way of contrast, the ortho-bridged $3^{+\bullet}$ showed essentially the same UV–vis bands, but the most prominent feature of the electronic spectrum was the additional presence of the very broad absorption band in the near-IR region with $\lambda_{\text{CR}} = 1600$ nm,³² the Gaussian band shape of which is confirmed in the inset (dotted line) to Figure 5A.³³ The band intensity, which was directly proportional to the concentration of $3^{+\bullet}$ and quite independent of added neutral mixed-valence donor **3**, confirmed its intramolecular character. Since the further selective oxidation of $3^{+\bullet}$ to the dication 3^{2+} was accompanied by the complete disappearance of only the near-IR band, it was assigned to the intervalence transition, similar to the charge-resonance (CR) bands observed with intermolecular dimer cation radicals such as **1** in Chart 1.³ The electronic spectrum of the mixed-valence cation radical $7^{+\bullet}$ comprised the sterically hindered (**S**) redox centers shown in Figure 5B is similar to that of the analogous $3^{+\bullet}$ containing **T** redox centers—with the sole exception that the intervalence band in the near-IR region was blue shifted to $\lambda_{\text{CR}} = 1100$ nm, as determined by Gaussian deconvolution (see Figure 5B, inset).

(29) See Lewis, Fraenkel, et al. in ref 1 and Kochi et al. in ref 4e and references therein.

(30) (a) Rathore, R.; Lindeman, S.; Kochi, J. K. *J. Am. Chem. Soc.* **1997**, *119*, 9393. (b) Hubig, S. M.; Rathore, R.; Kochi, J. K. *J. Am. Chem. Soc.* **1999**, *121*, 617. (c) Rathore, R.; Kochi, J. K. *J. Org. Chem.* **1995**, *60*, 4399.

(31) Heinzer, J. Quantum Chemistry Program Exchange 209, as modified by P. A. Pettillo and R. F. Ismagilov. We thank Prof. S. F. Nelsen for providing us with a copy of this program.

(32) (a) Compare with the near-IR bands observed in the phenylene-bridged $2a^{+\bullet}$ by Lindeman et al. in ref 9a. (b) Furthermore, the solid-state spectra of $3^{+\bullet}\text{SbCl}_6^-$, $4^{+\bullet}\text{SbCl}_6^-$, and $6^{+\bullet}\text{SbCl}_6^-$ are essentially the same as those in solution (see Figure S2 in the Supporting Information).

(33) (a) Careful scrutiny of the UV–vis spectra of $3^{+\bullet}$ and $7^{+\bullet}$ in Figure 5 reveals a minor component with $\lambda_{\text{max}} 900$ – 1000 nm. Since such absorptions are absent in the meta- and para-bridged $4^{+\bullet}$ and $5^{+\bullet}$, it is unlikely to derive from the br-to- $S^{+\bullet}$ charge transfer. (b) Strong absorptions in this spectral region are commonly observed (as an impurity?) when aromatic cation radicals are exposed to their parent donor and thus merit further study.

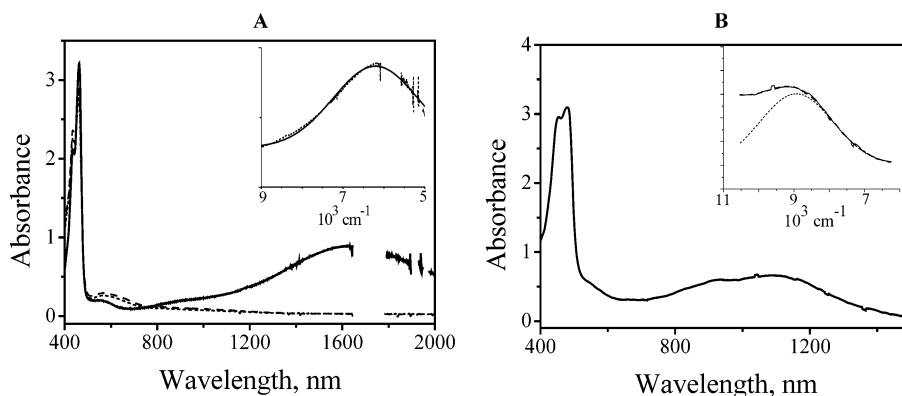
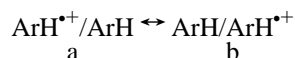


Figure 5. (A) Electronic spectra of mixed-valence cation radicals $3^{+\bullet}$ (solid line) and $4^{+\bullet}$ (black dashed line) and their mononuclear model $6^{+\bullet}$ (gray dashed line) in dichloromethane solution, showing the prominent absorption in the near-IR region of $3^{+\bullet}$ only. (B) Electronic spectrum of the sterically hindered cation radical $7^{+\bullet}$ with the prominent absorption in the near-IR region.³³ Insets: Gaussian deconvolution of the low-energy absorptions of $3^{+\bullet}$ (A) and $7^{+\bullet}$ (B).

Discussion

The intermolecular dimer cation radicals of aromatic donors such as **1** (Chart 1) can be characterized by the pair of equivalent valence-bond structures shown in Chart 5, in accord with the Badger–Brocklehurst designation of their diagnostic optical transitions as *charge resonance*.³ The wide separation of $d_D \approx 3.2$ Å between the noncovalently bonded aromatic moieties in such cationic paramagnetic associates necessarily limits the conceptual electron exchange or hole hopping in Chart 5 to a *through-space* process—the mechanism of which has heretofore eluded detailed elucidation, owing to their highly transient character when generated via diffusional encounters.

Chart 5



I. Through-Space Electron Delocalization in Mixed-Valence Cation Radicals. The successful isolation of the mixed-valence cation radical $3^{+\bullet}$ with the bridged aromatic redox centers (**T** = 2,5-dimethoxy-*p*-tolyl) allows us the opportunity now to examine the structural properties of the cofacial redox centers responsible for the mechanism of the electron exchange or hole hopping by the application of four *independent* experimental probes, which we individually describe as follows.

A. Splitting of the Oxidation Potentials (ΔE) for Mixed-Valence Donors. The multiple electron transfer from a mixed-valence donor such as the *o*-xylylene-bridged **3** defines the comproportionation/disproportionation equilibrium. The Gibbs free-energy change ΔG_{com} for eq 6 is given by the magnitude of the potential splitting, $\Delta E = E_{1/2}(1) - E_{1/2}(2)$, as evaluated by the transient electrochemical data in Table 1 so that $\Delta G_{\text{com}} = F\Delta E$. Such a free-energy change is determined^{18,19,34} as the sum of statistical, electrostatics, and inductive terms and by the resonance stabilization ΔG_r , which is expressed as $\Delta G_r = -2H^2/\lambda$ where H is the critical electron coupling element

(34) (a) Sutin, N. *Prog. Inorg. Chem.* **1983**, *30*, 441. (b) Brunschwig, B. S.; Sutin, N. Reflections on the two-state electron-transfer model. In: *Electron Transfer in Chemistry*; Balzani, V., Ed.; Wiley: New York, 2001; Vol. 2, p 583. (c) Brunschwig, B. S.; Sutin, N. *Coord. Chem. Rev.* **1999**, *187*, 233. (d) Sutin, N. *Adv. Chem. Phys.* **1999**, *106*, 7. (e) We recognize that the two-state model for electron transfer is based on orthogonal initial and final diabatic states;^{10,34a} the extent to which there is orbital overlap between cofacial aromatic redox centers as in $3^{+\bullet}$ (with $d_D \approx 3.2$ Å) could violate this theoretical restriction.^{51b}

Table 4. Electronic Spectra of Mixed-Valence Cation Radicals and Their Mononuclear Models^a

MVCR	λ (ε)
$3^{+\bullet}$	438 (4.7), 464 (4.8), 600 sh, 850 sh, 1600 (1.1)
$4^{+\bullet}$	438 (5.6), 462 (5.8), 600 sh
$5^{+\bullet}$	438 (5.6), 462 (5.8), 600 sh
$6^{+\bullet}$	438 (5.7), 462 (5.9), 600 sh
$7^{+\bullet}$	440 (5.2), 471 (5.5), 600 sh, 900 sh, 1120 (0.32)
$8^{+\bullet}$	440 (5.0), 473 (5.4), 600 sh
$9^{+\bullet}$	440 (5.1), 468 (5.4), 600 sh, 732 sh, 807 (0.48), 913 (0.36)
$10^{+\bullet}$	440 (5.0), 470 (5.5), 600 sh, 728 (0.18), 797 (0.41), 933 (0.17)

^a Band maxima λ in nm, with extinction coefficients, ϵ , in $10^3 \text{ M}^{-1} \text{ cm}^{-1}$.

Table 5. Estimation of the Electronic Coupling Elements in Organic Mixed-Valence Cation Radicals via the Mulliken–Hush Formalism (from the Intervalence Band) and Cyclic Voltammetry Data

MV-CR	ν_{IV} , 10^3 cm^{-1}	$\Delta\nu_{IV}$, 10^3 cm^{-1}	ϵ , $10^3 \text{ M}^{-1} \text{ cm}^{-1}$	r , Å	H_{IV} , 10^3 cm^{-1}	ΔE^{ox} , V	H_{TD} , 10^3 cm^{-1}
$3^{+\bullet}$	6.25	2.1	1.1	3.2 ^d	0.76	0.16	2.00
$7^{+\bullet}$	8.93	2.1	0.32	4.0 ^e	0.40		

^a Band full width at half-height. ^b Calculated with the Mulliken–Hush equation.³⁸ ^c Evaluated from $\Delta E = -\Delta G/F = 2H^2/(\lambda F)$. ^d Interplanar distance from X-ray crystallography. ^e Average interplanar distance from molecular mechanics calculations.

between the $\text{T}^{\bullet+}/\text{T}$ redox centers in the mixed-valence cation radical $3^{+\bullet}$ and λ is the Marcus reorganization energy.⁹ If we assume for the moment that the resonance interaction is the major contributor to the mixed-valence cation radical $3^{+\bullet}$, the electronic coupling can be directly evaluated from ΔG_{com} (vide supra), and the thermodynamics results are listed as H_{TD} in the last column of Table 5.³⁵

B. Geometrical Changes and the Charge Distribution (q_i) for the Redox Centers in Mixed-Valence Cation Radicals. X-ray crystallographic analyses of the mixed-valence donor **3** and its cation radical $3^{+\bullet}$ identify three structural features unique to this ortho-bridged system. *First*, the quantitative transformation of the overall anti conformation of the redox centers in **3** (Figure 1A) to the highly ordered syn conformation (Figure 1B) accompanies its oxidative transformation to $3^{+\bullet}$. Since the

(35) Note that H_{TD} evaluated from the electrochemical data is expected to represent an upper limit to the intrinsic electronic coupling element, owing to the neglect of the other energy terms described above.

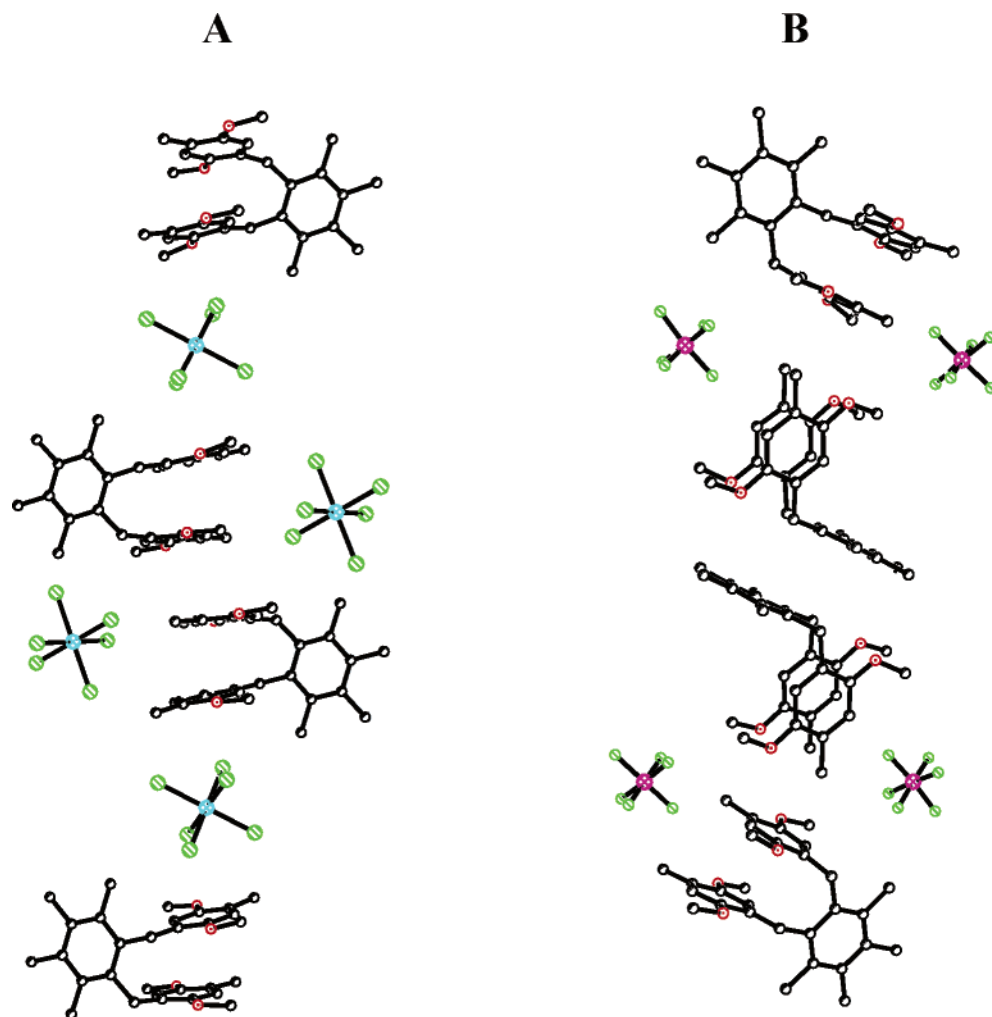


Figure 6. Crystal packings in the unit cells of the mixed-valence cation-radical salts $3^{+\bullet}\text{SbCl}_6^-$ (A) and $3^{+\bullet}\text{PF}_6^-$ (B).

different conformations extant in the mixed-valence donors such as **3** are not strongly differentiated, though the anti conformation is slightly favored,³⁶ the marked syn/anti conformational change observed upon one-electron oxidation of **3** is consistent with even a modest energy gain such as that contributed from ΔG_r . In other words, the resonance interaction of $\text{T}^{\bullet+}/\text{T}$ centers as formalized in Chart 5 can represent a major contributor to the formation/stabilization of the mixed-valence cation radical $3^{+\bullet}$ that is unique to the ortho-bridged but not the meta/para isomers.

Second, the major configurational change in the redox center attendant upon the formation of the mixed-valence cation radical, as measured by the increase in its quinonoidal character, quantitatively relates to the charge q_i residing on the **T** centers-(s). The experimental value of $q_i = +0.5, +0.5$ in $3^{+\bullet}\text{PF}_6^-$ (Table 3) indicates that complete electron delocalization is achieved between both redox centers, as predicted by the charge-resonance character described in Chart 5. *Third* and most important is the cation-dependent nature of q_i —being 0.9, 0.1 in $3^{+\bullet}\text{SbCl}_6^-$. Such a significant difference in the charge distribution in the pair of redox centers of $3^{+\bullet}$ is readily accommodated by the distinctive location of PF_6^- and SbCl_6^- in the unit cell (Figure 6). In particular, SbCl_6^- is asymmetrically poised over a single redox center, whereas both centers are

symmetrically perturbed by PF_6^- so that electrostatic polarization alone can account for the complete electron/charge delocalization observed in $3^{+\bullet}\text{PF}_6^-$ crystals. Be that as it may, the crystalline counterion effects clearly show that the electron/charge distribution in the resonance stabilization of the ortho-bridged $3^{+\bullet}$ is highly sensitive to external electrostatic influences—as stereoselectively imposed by the counterions in the rigid solid-state lattice.

C. Equivalent Number and Hyperfine Splitting of Paramagnetic Centers in Mixed-Valence Cation Radicals. The unique sets of equivalent protons in the redox center **T** provides an alternative probe for electron/charge delocalization in the mixed-valence cation radical. Accordingly, the doubling of the number and halving the proton splittings in the ortho-bridged $3^{+\bullet}$ relative to those in the mononuclear model $6^{+\bullet}$ indicate that both of the **T** centers on the ESR time scale bear equally the same odd-electron density—consistent with their juxtaposition and resonance stabilization as provided by the transient electrochemical and X-ray crystallographic results. Moreover, this conclusion is unique to the ortho-bridged cation radical, since cyclic voltammetry (Table 1), X-ray crystallography (Table 2), and ESR spectroscopy (Table 3) for the meta and para isomers show no such unusual behavior.

D. Intervalence (Charge-Resonance) Transitions in Mixed-Valence Cation Radicals. Electronic (UV–vis) spectroscopy

(36) For a description of the conformational syn/anti equilibrium, see the Experimental Section.

provides the fastest time resolution for probing electron delocalization in mixed-valence cation radicals, and the observation of the unique near-IR absorption band in the ortho-bridged cation radical $3^{+\bullet}$, but not in the meta and para isomers $4^{+\bullet}$ and $5^{+\bullet}$, bears direct relationship to the charge-resonance bands reported by Badger, Brocklehurst, and co-workers³ for the *intermolecular* dimer cation radicals such as **1** in Chart 1. Furthermore, the spectral observation of the charge-resonance band is even possible in the sterically hindered mixed-valence cation radical $7^{+\bullet}$ (entry 5), despite its very short lifetime on the ESR time scale, as indicated by the absence of the hyperfine doubling (Table 3, entry 8). Accordingly, let us examine how the Mulliken formalism³⁷ of charge-transfer transition, as theoretically developed by Hush,³⁸ can be applied to the charge-resonance bands for the ortho-bridged cation radicals such as $3^{+\bullet}$ and $7^{+\bullet}$.

II. Intramolecular Electron Transfer in Mixed-Valence Cation Radicals. A. Application of Mulliken–Hush Theory.

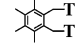
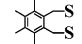
For mixed-valence complexes (particularly with transition-metal redox centers), Hush identified the intervalence (charge-transfer) transition to reflect the electronic coupling element according to the relationship^{34,38} $H_{IV} = 0.0206(\nu_{\max}\Delta\nu_{1/2}\epsilon)^{1/2}/r$, where ν_{\max} and $\Delta\nu_{1/2}$ are the maximum and full width at half-heights of the near-IR absorption band (in cm^{-1}), ϵ is the molar extinction coefficient at the absorption maximum (in $\text{M}^{-1}\text{cm}^{-1}$), and r is the effective separation of redox centers in the mixed-valence complex (in Å). The direct application of the intervalence spectral parameters in Table 4 and the separation parameter from the X-ray crystallographic analysis for the ortho-bridged mixed-valence cation radicals $3^{+\bullet}$ and $7^{+\bullet}$ to the Hush equation yields the values of the electronic coupling element H_{IV} in Table 5, column 6.

We note that the values of the electronic coupling element H_{IV} in Table 5 (column 6) determined from the intervalence charge-resonance transition with the aid of the Mulliken–Hush formalism^{37,38} are significantly smaller than H_{TD} evaluated from the thermodynamic data in Table 1 (column 8). Part of this discrepancy is doubtless due to the neglect of other (energy) terms in the thermodynamic treatment, as described above; however, the question does arise as to whether Mulliken–Hush theory is applicable to through-space electron transfer (ET) of the type extant in the *o*-xylylene-bridged cation radical, as presented in the previous section. The principal test of the validity of such a theoretical formulation to identify the optical charge-resonance transitions in mixed-valence cation radicals is the direct comparison of the predicted rates of intramolecular electron transfer with the experimental rates obtained independently,³⁹ as follows.

B. Theoretical and Experimental Comparison of (Electron-Transfer) Rates.

According to Marcus–Hush theory,⁴⁰ the

Table 6. Comparison of Experimental (ESR) and Calculated (MH) Intramolecular Electron-Transfer Rate Constants in Bridged (Mixed-Valence) Cation Radicals

MVCR	ΔG^* , ^a kcal/mol	$k_{\text{ET}}(-80^\circ\text{C})$, s^{-1}		$k_{\text{ET}}(+30^\circ\text{C})$, s^{-1}	
		MH ^b	ESR ^c	MH ^b	ESR ^c
$3^{+\bullet}$ 	2.6	1×10^9	$>10^9$	4×10^9	$>10^9$
$7^{+\bullet}$ 	5.4	2×10^6 ^d	5×10^6 ^d	2×10^7 ^e	4×10^7 ^e

^a From $\Delta G^* = (\lambda - 2H_{\text{MH}})^2/(4\lambda)$. ^b Calculated from $k_{\text{ET}} = 10^{12} \exp(-\Delta G^*/RT)$. ^c Evaluated from ESR line broadening. ^d At -60°C . ^e At -20°C .

intramolecular first-order rate constant for electron transfer within the mixed-valence complex can be evaluated as $k_{\text{ET}} = k\nu_n \exp(-\Delta G^*/RT)$, where k is the electronic transmission coefficient, ν_n is the nuclear vibration frequency related to electron transfer, and ΔG^* is the free energy of activation for electron transfer.³⁴ When the electronic coupling is sufficiently strong (as given in Table 5), electron transfer is adiabatic with $k \approx 1$, and the activation barrier is given by³⁴

$$\Delta G^* = (\lambda - 2H)^2/4\lambda \quad (8)$$

The combination of the reorganization energy λ , the electron coupling element H_{IV} obtained from the intervalence transition in Table 5, and $\nu_n = 10^{12} \text{ s}^{-1}$ ⁴¹ leads to the first-order rate constants in Table 6 (columns 3 and 5). The experimental first-order rate constants for the mixed-valence cation radicals $3^{+\bullet}$, with a pair of **T** centers, and $7^{+\bullet}$, with a pair of sterically hindered **S** centers, are also included in Table 6, columns 4 and 6.

It is noteworthy that the experimental first-order rate constants in Table 6 (columns 4 and 6) for the intramolecular electron transfer obtained from the ESR line-broadening studies agree satisfactorily with the predictions of Marcus–Hush theory (columns 3 and 5). *First*, the fast electron-transfer rate constant of $k_{\text{ET}} > 10^9 \text{ s}^{-1}$ for $3^{+\bullet}$ at all accessible temperatures derives from the very low barrier of $\Delta G^* = 2.6 \text{ kcal mol}^{-1}$ predicted by Marcus–Hush theory; this is in accord with the absence of the experimental line broadening at the upper limit of the ESR time scale. The latter thus limits the half-life for electron transfer between **T**⁺/**T** centers in the ortho-bridged cation radical to $\tau_{\text{ET}} < 10^{-9} \text{ s}^{-1}$ —in complete accord with the conclusion derived from the experimental probes (vide supra) explored in this study. *Second*, the significantly slower rate of intramolecular electron exchange in $7^{+\bullet}$ (with the sterically hindered **S**⁺/**S** centers) allows the quantitative application of the ESR line-broadening methodology. Indeed, the results for $7^{+\bullet}$ in Table 6 (column 6) obtained from the line-broadening study at high temperature (30°C) agree easily within an order of magnitude of the predictions of Marcus–Hush theory (column 5). *Third*, at the other extreme of low temperature (-80°C), the first-order rate constant near 10^6 s^{-1} for $7^{+\bullet}$ borders the lower limit too closely to be reliably measured by their ESR line-broadening. Nonetheless, the estimates listed in Table 6 (column 4) generally are in accord with the predicted rate constant based on $\Delta G^* = 5.4 \text{ kcal mol}^{-1}$ calculated from eq 9 and the value of H_{IV} in Table 5.

(40) (a) Marcus, R. A. *Angew. Chem., Int. Ed. Engl.* **1993**, *32*, 1111. (b) Marcus, R. A. *Discuss. Faraday Soc.* **1960**, *29*, 21. (c) Marcus, R. A. *J. Phys. Chem.* **1963**, *67*, 853. (d) Marcus, R. A. *J. Chem. Phys.* **1965**, *43*, 679. (e) Marcus, R. A.; Sutin, N. *Biochim. Biophys. Acta* **1985**, *811*, 265.

(37) (a) Mulliken, R. S. *J. Am. Chem. Soc.* **1952**, *74*, 811. (b) Mulliken, R. S.; Person, W. B. *Molecular Complexes*; Wiley: New York, 1969.

(38) (a) Hush, N. S. *Z. Electrochem.* **1957**, *61*, 734. (b) Hush, N. S. *Trans. Faraday Soc.* **1961**, *57*, 557. (c) Hush, N. S. *Prog. Inorg. Chem.* **1967**, *8*, 391. (d) Hush, N. S. *Electrochim. Acta* **1968**, *13*, 1005. (e) We have evaluated the separation parameter r in the Hush equation for H_{IV} from the molecular geometry on the basis of either the X-ray crystallographic parameter or molecular mechanics computations.^{38g} Such assignments are at best only estimates of the molecular redox centers as complex as **T**, **S**, and **P**.^{38f} However, even substantial deviations are not sufficient to qualitatively change the conclusions. (f) See also: Nelsen, S. F.; Newton, M. D. *J. Phys. Chem.* **2000**, *104*, 10023. (g) HyperChem Release 5.11 Pro for Windows Molecular Modeling System; Hypercube, Inc., 1999.

(39) For previous examples of the application of such a test, see: Elliot, C. M.; Derr, D. L.; Matyushov, D. V.; Newton, M. D. *J. Am. Chem. Soc.* **1998**, *120*, 11714. See also Nelsen and co-workers in ref 11.

C. Electron-Density Distribution between Redox Centers in Mixed-Valence Cation Radicals. Substantial changes in the ground-state distribution of the electron density of the redox centers in mixed-valence cation radicals and thus their molecular structures are predicted when the magnitude of the electronic coupling element between redox centers is substantial relative to the reorganization energy.³⁴ In terms of the ET reaction coordinate, such increasing values of H/λ result in the gradual shift of the reactant minimum from (a) $X_{\min} = 0$ with $H = 0$, at which the charge distribution is +1.0/0 and the molecular structure corresponds to a pair of noninteracting \mathbf{T}^+/\mathbf{T} centers, to (b) $X_{\min} = 0.5$ with $H \geq \lambda/2$, at which electron delocalization is complete so that both redox centers bear a +0.5 charge. As such, the changing values of X_{\min} reflect partial transfer of electron density and translate into structural changes in the redox centers—which in the case of the highly variable \mathbf{T} center is represented by partial quinonoid distortion (see Table 2).

For the ortho-bridged mixed-valence cation radical $\mathbf{3}^{+}$, the theoretical estimates of X_{\min} evaluated from the relationship³⁴ $X_{\min} = 1/2[1 - (1 - 4H^2/\lambda^2)^{1/2}]$ are $X_{\min} = 0.02$ based on H_{IV} and $X_{\min} = 0.12$ based on H_{TD} in Table 5, columns 6 and 8, respectively. Such small values of X_{\min} ³⁵ correspond to only minor changes in both \mathbf{T}^+ and \mathbf{T} centers relative to those in noninteracting redox sites;⁴² this charge distribution is experimentally observed in the crystalline hexachloroantimonate salt of $\mathbf{3}^{+}$ (see Table 2, third entry). Thus, $\mathbf{3}^{+}\text{SbCl}_6^-$ clearly resides in the class II (localized) category according to the Robin–Day classification of mixed-valence systems.⁴³

On the other hand, the experimental X-ray structural analysis of the crystalline hexafluorophosphate salt of $\mathbf{3}^{+}$ establishes an equal charge distribution between both redox centers. Generally speaking, such an unusual charge distribution in crystalline $\mathbf{3}^{+}\text{PF}_6^-$ can be attributed to (a) crystallographic statistical disorder, (b) dynamic disorder arising from fast electron transfer, or (c) complete static charge delocalization between redox sites. The absence of crystallographic symmetry²⁵ allows alternative a to be excluded, and the observation of Robin–Day class II behavior in the structurally equivalent $\mathbf{3}^{+}\text{SbCl}_6^-$ salt strongly disfavors alternative c. Accordingly, we conclude that the fast intramolecular process observed for $\mathbf{3}^{+}$ with $\tau < 10^{-9}$ s⁻¹ must derive from the very low activation barrier of $\Delta G^* = 2.6$ kcal mol⁻¹ for electron exchange (see eq 7), as predicted by the large electronic coupling element H_{IV} in Table 5. The latter is structurally consistent with the close cofacial separation between \mathbf{T}^+/\mathbf{T} centers of $d_{\text{D}} = 3.2$ Å evaluated by X-ray crystallographic analysis of both $\mathbf{3}^{+}\text{SbCl}_6^-$ and $\mathbf{3}^{+}\text{PF}_6^-$ salts. This spatial situation is considerably less

favorable in the analogous mixed-valence cation radical $\mathbf{7}^{+}$, in which steric encumbrance by annulation precludes the same close approach of the \mathbf{S}^+/\mathbf{S} redox centers, resulting in almost halving of the H_{IV} values. Although we were unable to isolate crystalline salts of $\mathbf{7}^{+}$ for X-ray crystallographic analysis, preliminary molecular mechanics computations suggest a van der Waals distance of approximately 4.0 Å.^{38g} If so, the significant difference between the H_{IV} values for $\mathbf{3}^{+}$ and $\mathbf{7}^{+}$ suggest that the effectiveness of the through-space mechanism for electron exchange between redox centers in eq 8 drops off sharply with separation.⁴⁴

For a more comprehensive consideration of the distance dependence of intramolecular electron transfer in mixed-valence cation radicals, we now compare the *through-space* mechanism allowed by the *o*-xylylene-bridged cation radical $\mathbf{3}^{+}$ in Chart 3 with the *through-bridge* mechanism enforced by the rigid *p*-phenylene bridge in the mixed-valence cation radical $\mathbf{2a}^{+}$ in Chart 2.

III. Through-Space versus Through-Bond Electron Transfer in Mixed-Valence Cation Radicals. For the intramolecular electron exchange via the *through-space* mechanism,^{45,46} the redox centers \mathbf{T}^+/\mathbf{T} in the conformationally mobile cation radical $\mathbf{3}^{+}$ are disposed *cofacially*, as depicted in Figure 1B for conformer $\mathbf{3b}$ described in Chart 5 at an interplanar separation of $d_{\text{D}} = 3.2$ Å. For the contrasting *through-bond* mechanism applicable to the structurally rigid cation radical $\mathbf{2a}^{+}$, the same \mathbf{T}^+/\mathbf{T} centers lie coplanar and are linearly connected end to end by the rigid *p*-phenylene bridge, which separates the redox centers by ~ 8 Å. For the comparison of the *through-space/through-bond* electronic interactions of the redox centers in mixed-valence cation radicals, we focus on three different facets as follows.

A. Our initial study⁹ of intramolecular electron exchange in the mixed-valence cation radical $\mathbf{2a}^{+}$ followed from earlier studies that employed the same *p*-phenylene bridge in various mixed-valence cation radicals with redox centers derived from alkyldiazines, phenylenediamines, triarylaminines, and related N-centered donors.^{11,12c,d} In those cases, the quantitative analysis of the intervalence charge-transfer bands by application of the Marcus–Hush two-state model to the *p*-phenylene-bridged cation radicals⁴⁷ afforded intramolecular first-order rate constants that agreed with experimental values obtained independently by dynamic ESR measurements. If such impressive agreements serve as a valid test of the two-state model to predict intramolecular electron exchanges generally for mixed-valence cation radicals with *p*-phenylene bridges, then the spectral analysis of the intervalence charge-resonance transition in our cation radical $\mathbf{2a}^{+}$ by the same Marcus–Hush methodology, as presented in Table 7, entry 2,⁴⁸ should serve to validate the predicted rate constant in column 7 for the *through (br)-bond* electron transfer between \mathbf{T}^+/\mathbf{T} centers. Indeed, the calculated value of H_{IV} in column 5 for the para-bridged $\mathbf{2a}^{+}$ from the intervalence band

(41) For this study, we have simply taken ν_n to be uniformly 10^{12} s⁻¹, the same value as previously used for the description of electron transfer in phenylene-bridged organic mixed-valence cation radicals⁹ with similar redox centers, and this value of ν_n agrees reasonably well with that employed in the kinetics evaluation of the intermolecular anion-radical self-exchange.^{41b} (b) See Ganesan et al. in ref 4g.

(42) Note that the value of $X_{\min} = 0.02$ is beyond X-ray structural analysis to readily distinguish from $X_{\min} = 0$, even with the best accuracy provided by this method.

(43) (a) Robin, M. B.; Day, P. *Adv. Inorg. Chem. Radiochem.* **1967**, *10*, 247. (b) For the application of the Robin–Day classification to organic mixed-valence systems, see Lambert et al. in ref 12c and Lindeman et al. in ref 9a. (c) To the extent to which the mixed-valence cation radical falls from the class III (delocalized) to the class II (localized) category, the charge-resonance designation should be replaced by charge transfer. (d) Although a reviewer has suggested that electrostatic polarization could induce an asymmetric structure of a class III mixed-valence cation radical, the evaluation of H and λ in Table 5 indicates that $\mathbf{3}^{+}\text{SbCl}_6^-$ belongs in class II.

(44) In addition, the cofacial \mathbf{S}^+/\mathbf{S} centers in $\mathbf{7}^{+}$ are offset.

(45) Note that the absence of electronic interaction between \mathbf{T}^+/\mathbf{T} centers in the meta- and para-bridged cation radicals $\mathbf{4}^{+}$ and $\mathbf{5}^{+}$ shows that the *through (br)-bond* mechanism also does not play a role in the ortho isomer $\mathbf{3}^{+}$.

(46) For previous studies on this type of through-space electronic interactions, see: Rathore, R.; Kochi, J. K. *Can. J. Chem.* **1999**, *77*, 913.

(47) As applied to mixed-valence cation radicals, the resonance “structures” a and b in Chart 5 relate directly to the initial and final diabatic states in the two-state model for electron transfer.

(48) Data taken from Lindeman et al. in ref 9a.

Table 7. Comparison of the Electron-Transfer Parameters in Mixed-Valence Cation Radicals via Through-Bond and Through-Space Interactions

MVCR	Structure	ΔE , V	λ ($=\nu_{IV}$) 10^3 cm^{-1}	H_{IV} , 10^3 cm^{-1}	q_i	ΔG^* , kcal/mol	k_{ET}^{ESR} , s^{-1}
3^{•+}		0.16	6.25	0.76	0.9(0.5)	2.6	$>10^9$
2a^{•+}		0.11	6.37	0.76	0.8	2.6	$>10^9$
7^{•+}		a	8.93	0.40	-	5.4	4×10^{10}
2b^{•+}		a	6.79	0.43	1	3.7	2×10^{10}

^a Broadened two-electron oxidation wave with $\Delta E \approx 0.02$ V. ^b At -40 °C. ^c At -100 °C, from ref 9.

correctly accounts for the very low activation energy ΔG^* for *through (br)-bond* electron transfer and the observed splitting of ΔE observed for the CV waves established experimentally. When the same two-state model methodology is applied to the intervalence charge-resonance band of ortho-bridged **3^{•+}** examined in this study, the calculated value of the electronic coupling element (Table 7, column 5) predicts the same kinetics behavior (compare entries 1 and 2) for *through-space* electron transfer from almost the same splitting of the CV wave; most importantly, it leads to the same values of λ_T for the reorganization energy (column 4), despite the widely divergent symmetry pattern of orbital overlap extant in **3^{•+}** vis á vis **2a^{•+}**. Accordingly, we conclude that both **3^{•+}** and **2a^{•+}** represent ground states with high degrees of electron delocalization between **T^{•+}/T** centers on the ESR time scale; this is in accord with X-ray structural analysis of the quinonoidal distortions and their particularly high degree of electrostatic polarizability by the accompanying negatively charged counterions—all independent of whether through-space or through-bond electron transfer pertains.

B. The further pursuit of the distance comparison is presented in Table 7, in which the *through-space* separation of the cofacial redox centers by steric encumbrance, as in cation radical **7^{•+}** containing the annulated **S^{•+}/S** pair, is considered in the context of the *through-bond* extension via the incorporation of another (br) link, as in the *p*-biphenylene-bridged **2b^{•+}** identified in Chart 2. In each case, the increased distance between the cofacial redox centers in **7^{•+}** by an incremental amount of only ~ 0.5 Å (relative to that in **3^{•+}**) and the larger linear separation of ~ 5 Å in **2b^{•+}** (relative to that in **2a^{•+}**) inflict more or less comparable diminutions in the values of the electronic coupling element (compare the third/fourth entries in Table 7). Most notably, the accompanying increases in the calculated reorganization energies (column 5) and activation energies (column 6) in both **7^{•+}** and **2b^{•+}** correctly predict the intramolecular first-order rate constants for the electron exchange k_{ET} , which have been independently confirmed by ESR line-broadening measurements.

C. We also evaluate the *through-space/through-bond* dichotomy⁴⁹ via the use of a different redox center, **P** (phenothiazinyl), in which the reorganization energy of $\lambda_P = 1 \times 10^4$ cm^{-1} is substantially larger than that of the redox center **T** or **S**.¹⁵ Despite this distinction, the analysis of the intervalence charge-resonance transitions with the aid of the two-state model provides a calculated value of the electron coupling element for the **P^{•+}/P** centers in the *o*-xylylene-bridged cation which is the same as that in the *p*-phenylene-bridged cation radical. As a result, the predicted activation energy and reorganization energy for through-space/through-bond electron transfer are

comparable and both are experimentally confirmed by (a) the splitting of the CV waves and (b) the intramolecular first-order rate constant evaluated by dynamic ESR measurements.^{15b}

Summary and Conclusions

The through-space versus through-bond pathways for intramolecular electron transfer between a pair of bridged aromatic redox centers are provided by the syntheses of the mixed-valence donors **3** and **2a** depicted in Charts 3 and 2, respectively.⁴⁹ Selective oxidation generates the mixed-valence systems with the pair of aromatic redox centers **Ar^{•+}/Ar** separated by a conformationally flexible *o*-xylylene bridge in **3^{•+}** and the rigid *p*-phenylene bridge in **2a^{•+}** to serve in this study as *through-space* and *through-bond* prototypes, respectively.

Through-space electron transfer is established in **3^{•+}** by the mutually syn conformations of **T^{•+}/T** centers that are cofacially separated by $d_D = 3.2$ Å, as determined by X-ray crystallographic analysis in Figure 2. Strong electronic interaction between such nonbonded aromatic centers is reminiscent of that extant in a dimer cation radical such as **1** in Chart 1 and previously evaluated by their pronounced “charge-resonance” absorption bands in the near-IR region.^{3,4} Independent measurements of the potential splitting in the cyclic voltammograms (Table 1), quinonoidal distortion of both **T^{•+}/T** centers by X-ray crystallographic analysis (Table 2), and the “doubling” of the ESR spectra (Table 3) all lead to the same conclusion of the effectiveness of the cofacial disposition of **Ar^{•+}/Ar** redox centers in intramolecular electron transfer. Strong electronic interaction between **T^{•+}/T** centers in **3^{•+}** lead to the first-order rate constant $k_{ET} > 10^9$ s^{-1} , as qualitatively deduced from ESR spectroscopy. Such fast electron-transfer rates with $k_{ET} = 4 \times 10^9$ s^{-1} also derive from Marcus–Hush theory as a result of the sizable electronic coupling element evaluated from the charge-resonance absorption band according to the Mulliken–Hush formalism. More to the point, the same treatment of the mixed-valence donor with the sterically hindered redox center **S** leads to cation radical **7^{•+}**, exhibiting substantially slower rates with $k_{ET} = 1.5 \times 10^7$ s^{-1} that are readily measured by quantitative ESR line-broadening studies; the *same* theoretical value of $k_{ET} = 1.3 \times 10^7$ s^{-1} derives from the application of the Marcus–Hush theory and the use of the electronic coupling element evaluated from the intervalence charge-resonance transition. Even more important is the magnitude of the Arrhenius activation energy of $E_a = 6.2$ kcal mol^{-1} from the ESR line broadening, which is close to the Gibbs activation free-energy change of $\Delta G^* = 5.4$ kcal mol^{-1} calculated from the Marcus–Hush equation (8) and the value of $H_{IV} = 400$ cm^{-1} evaluated from the intervalent (charge-resonance) band in Table 5.⁵⁰

Through (br)-bond electron transfer is enforced by the structurally rigid *p*-phenylene bond in the mixed-valence cation

(49) For some previous studies of the *through-space/through-bond* dichotomy, see: (a) Clayton, A. H. A.; Scholes, G. D.; Ghiggino, K. P.; Paddon-Row, M. N. *J. Phys. Chem.* **1996**, *100*, 10912. (b) Bell, T. D. M.; Jolliffe, K. A.; Ghiggino, K. P.; Oliver, A. M.; Shephard, M. J.; Langford, S. J.; Paddon-Row, M. N. *J. Am. Chem. Soc.* **2000**, *122*, 10661. (c) Koeberg, M.; de Groot, M.; Verhoeven, J. W.; Lokan, N. R.; Shephard, M. J.; Paddon-Row, M. N. *J. Phys. Chem. A* **2001**, *105*, 3417. (d) Pullen, S. H.; Studer-Martinez, S. L.; Edington, M. D.; Harris, A. L.; Long, A.; Baldwin, S. W.; Staab, H. A.; Simon, J. D. *J. Phys. Chem. A* **1999**, *103*, 10220. (e) Arimura, T.; Ide, S.; Suga, Y.; Nishioka, T.; Murata, S.; Tachiya, M.; Nagamura, T.; Inoue, H. *J. Am. Chem. Soc.* **2001**, *123*, 10744.

(50) Note that this direct comparison of experimental with theoretical barriers of electron transfer is independent of any ambiguity in our evaluation of the preexponential factor.⁴¹

radical $2a^{+}$ reported earlier.^{9a} Indeed, the four experimental probes for electronic interaction of T^{+}/T centers including (a) splitting of the CV wave, (b) quinonoidal distortion of T in the X-ray structure, (c) doubling of the ESR spectrum, and (d) pronounced intervalence absorption bands were characteristics that are all shared in common with the through-space interactions observed with mixed-valence cation radicals 3^{+} and 7^{+} (vide supra)—and the quantitative comparisons in entries 1 and 2 in Table 7 reinforce this direct correspondence. The same picture emerges from the experimental (first-order) rate constants k_{ET} measured by ESR line broadening in comparison with the computed results from Marcus–Hush theory using the electronic coupling element derived from the intervalence transition with the aid of the Mulliken–Hush formalism. Such a quantitative coherence of experimental results with theoretical calculations indicates that the two-state model may be reliably applied more generally to through-space electron transfer in other organic mixed-valence cation radicals;⁵¹ such a conclusion is strongly supported by our results with the phenothiazinyl (P) redox center in the direct comparison of through-space/through-bond mechanisms in intermolecular and intramolecular ET pathways.^{15b}

Experimental Section

Materials and Synthesis. 1,2,3,4-Tetramethylbenzene, 1,2,3,5-tetramethylbenzene, 1,2,4,5-tetramethylbenzene, pentamethylbenzene, benzyl bromide, iodobenzene, 1,4-diiodobenzene, silver perchlorate, calcium carbonate, paraformaldehyde, 37% hydrobromic acid, methylhydroquinone, and *tert*-butylhydroquinone (from Aldrich, Acros, and Alfa) were used without further purification. Dichloromethane, toluene, hexane, and tetrahydrofuran were purified according to published procedures.⁵² 1,2-Bis(bromomethyl)tetramethylbenzene, 1,3-bis(bromomethyl)tetramethylbenzene, and 1,4-bis(bromomethyl)tetramethylbenzene were prepared by bromomethylation of benzenes according to the literature.¹⁶ 4,5-Dimethyl-1,2-diiodobenzene was synthesized by iodination of *o*-xylene with I_2 .^{53a} The mononuclear model donor 1,4-dimethyl-2,5-dimethoxybenzene (**6**) was synthesized as described.⁹ 2,5-Dimethoxymethylbenzene, 2,5-dimethoxy-*tert*-butylbenzene, and 2,5-diethoxybutylbenzene were synthesized by the alkylation of hydroquinones with dialkyl sulfates.^{53b} 1,4-Dimethoxy-5,8-methanotetrahydronaphthalene and 1,4-dimethoxy-2-methyl-5,8-methanotetrahydronaphthalene (**8**) were obtained in four steps as described earlier.^{30c} The neutral precursors of tris(2,4-dibromobenzene)amine, tris(4-bromobenzene)amine, and their radical cations (MG^{+}) as hexachloroantimonate and hexafluorophosphate salts were prepared according to the literature procedure.⁵⁴ All of the compounds prepared were characterized by 1H NMR, ^{13}C NMR, MS, melting points, and elemental analysis. The methylene-bridged alkyhydroquinones were readily prepared in two steps. For example, 1,2,3,4-tetramethylbenzene was bromomethylated with hydrogen bromide and formaldehyde in acetic acid to give 1,2-

bis(bromomethyl)tetramethylbenzene.¹⁶ Then 2,5-dimethoxytoluene was arylmethylated¹⁷ with 1,2-bis(bromomethyl)tetramethylbenzene in anhydrous benzene in the presence of silver perchlorate as a promoter and calcium carbonate as the acid scavenger to afford **3** in 47% yield.

1,2-Bis(2,5-dimethoxy-4-methyltolyl)tetramethylbenzene (3): mp 183–185 °C; 1H NMR ($CDCl_3$) δ 6.64 (s, 2H), 6.17 (s, 2H), 3.86 (s, 4H), 3.78 (s, 6H), 3.53 (s, 6H), 2.28 (s, 6H), 2.19 (s, 6H), 2.12 (s, 6H); ^{13}C NMR ($CDCl_3$) δ 152.1, 151.3, 134.7, 133.1, 127.8, 124.4, 120.0, 113.4, 112.9, 56.5, 56.1, 29.7, 16.8, 16.7, 15.8; MS (m/e) 463 ($M^+ + 1$, 22), 462 (M^+ , 75), 297 (37), 279 (100). Anal. Calcd for $C_{30}H_{38}O_4$: C, 77.92; H, 8.23. Found: C, 77.84; H, 8.28.

1,4-Bis(2,5-dimethoxy-4-methyltolyl)tetramethylbenzene (5): mp 191–192 °C; yield 43%; 1H NMR ($CDCl_3$) δ 6.78 (s, 2H), 6.21 (s, 2H), 4.09 (s, 4H), 3.95 (s, 6H), 3.56 (s, 6H), 2.27 (s, 6H), 2.21 (s, 12H); ^{13}C NMR ($CDCl_3$) δ 150.1, 150.5, 133.3, 132.2, 125.7, 123.2, 111.9, 110.8, 55.1, 54.9, 28.8, 15.6, 15.0. MS (m/e) 463 ($M^+ + 1$, 34), 462 (M^+ , 100), 297 (49), 279 (31). Anal. Calcd for $C_{30}H_{38}O_4$: C, 77.92; H, 8.23. Found: C, 78.17; H, 8.21.

1,3-Bis(2,5-dimethoxy-4-methyltolyl)tetramethylbenzene (4): mp 180–181 °C; yield 45%; 1H NMR ($CDCl_3$) δ 6.69 (s, 2H), 6.13 (s, 2H), 3.99 (s, 4H), 3.87 (s, 6H), 3.46 (s, 6H), 2.26 (s, 3H), 2.19 (s, 6H), 2.18 (s, 6H), 2.04 (s, 3H); ^{13}C NMR ($CDCl_3$) δ 150.6, 150.1, 133.0, 132.9, 132.8, 131.6, 125.7, 123.3, 111.9, 111.1, 55.4, 54.9, 28.7, 15.8, 15.7, 15.3, 14.9; MS (m/e) 463 ($M^+ + 1$, 34), 462 (M^+ , 100), 297 (49), 279 (31). Anal. Calcd for $C_{30}H_{38}O_4$: C, 77.92; H, 8.23. Found: C, 78.10; H, 8.17.

1,2-Bis(1,4-dimethoxy-5,8-methano-5,6,7,8-tetrahydronaphthalene-2-methylenyl)tetramethylbenzene (7): mp 135–136 °C; yield 21%; 1H NMR ($CDCl_3$) δ 5.92 (s, 2H), 3.90 (s, 4H), 3.71 (s, 6H), 3.53 (s, 6H), 2.25 (s, 6H), 2.12 (s, 6H), 1.87 (m, 4H), 1.67 (d, $J = 8.4$ Hz, 2H), 1.44 (d, $J = 8.4$ Hz, 2H), 1.12 (m, 4H); ^{13}C NMR ($CDCl_3$) δ 148.8, 145.6, 139.8, 134.5, 133.9, 133.0, 132.9, 131.1, 109.1, 60.7, 56.2, 56.1, 48.8, 40.9, 39.6, 30.0, 27.0, 26.6, 16.8.

1,2-Bis(2,5-dimethoxy-4-*tert*-butyltolyl)tetramethylbenzene (9): mp 179–181 °C; yield 19%; 1H NMR ($CDCl_3$) δ 6.75 (s, 2H), 6.17 (s, 2H), 3.87 (s, 4H), 3.78 (s, 6H), 3.48 (s, 6H), 2.25 (s, 6H), 2.10 (s, 6H), 1.33 (s, 18H); ^{13}C NMR ($CDCl_3$) δ 152.4, 150.4, 135.8, 134.1, 132.9, 127.2, 113.6, 109.2, 55.9, 55.8, 34.6, 28.7, 28.4, 16.8.

1,2-Bis(2,5-dimethoxy-4-*tert*-butyl-*p*-tolyl)tetramethylbenzene (10): mp 194–195 °C; yield 17%; 1H NMR ($CDCl_3$) δ 6.76 (s, 2H), 6.17 (s, 2H), 3.94 (q, $J = 7.2$, 4H), 3.86 (s, 4H), 3.66 (q, $J = 7.2$, 4H), 2.25 (s, 6H), 2.19 (s, 6H), 2.11 (s, 6H), 1.34 (s, 18H), 1.29 (t, $J = 9.6$, 12H); ^{13}C NMR ($CDCl_3$) δ 151.6, 149.8, 135.7, 134.5, 132.9, 132.8, 127.6, 113.6, 111.2, 64.6, 63.8, 34.5, 29.8, 29.4, 16.8, 16.8, 15.0, 14.8.

Conformational Equilibrium of Mixed-Valence Donor 3. Theoretical computations with Spartan software⁵⁵ indicated that the energies of the syn and anti conformers of **3** were rather close, although the energy of the syn conformer was about 2 kcal/mol higher than that of the anti conformer. The thermodynamics of the syn/anti equilibrium were experimentally studied by NMR spectroscopy, and Table S1 in the Supporting Information presents the chemical shifts of different sets of protons of **3** measured in the temperature range from +20 to –80 °C. The data indicated the upfield shift of the positions of all the chemical groups with increasing temperature, and the most prominent changes were related to the methylene bridge protons. On the basis of literature data,⁵⁶ such spectral changes were assigned to the shift of conformational equilibrium of **3** in eq 1—the temperature decrease being accompanied by a shift of the equilibrium to the energetically preferred anti conformation. On the basis of values of the chemical shifts of methylene (bridge) protons (most sensitive to conformational changes), the anti/syn equilibrium constant $K = [anti-3]/[syn-3]$ was calculated

(51) (a) Provided due cognizance is presently taken of the rigorous definitions of the separation parameter^{38c} and the preexponential factor⁴¹ for reliable computations of the Mulliken–Hush (MH) electronic coupling element, as described herein. Nonetheless, the ability of the two-state model to utilize the intervalence absorption bands to correctly predict the electron-transfer rates of mixed-valence cation radicals 3^{+} and 7^{+} underscores its utilitarian value for further use. (b) We hope that ongoing collaborative interactions with M. D. Newton will provide theoretical guidelines for critically assessing the quantitative application of the two-state model to mixed-valence cation radicals such as 3^{+} involving orbital overlap of juxtaposed (cofacial) redox centers.

(52) Perrin, D. D.; Armarego, W. L. F.; Perrin, D. R. *Purification of Laboratory Chemicals*, 2nd ed.; Pergamon: New York, 1980.

(53) (a) Hart, H.; Harada, K.; Du, C.-J. *J. Org. Chem.* **1985**, *50*, 3104. (b) Hiers, G. S.; Hager, F. D. *Organic Syntheses*; Wiley: New York, 1932; Collect. Vol. 1, p 58.

(54) Bell, F. A.; Ledwith, A.; Sherrington, D. C. *J. Chem. Soc. C* **1969**, 2719. Also see: Connelly, N. G.; Geiger, W. E. *Chem. Rev.* **1996**, *96*, 877 and references therein.

(55) PC Spartan MM3 Plus V; 2.0 Wavefunction, Inc., Irvine, CA, 1999.

(56) Compare: (a) Dix, D. T.; Fraenkel, G.; Karnes, H. A.; Newman, M. S. *Tetrahedron Lett.* **1966**, *5*, 517. (b) Jensen, F. R.; Bushweller, C. H. In *Advances in Alicyclic Chemistry*; Hart, H., Karabatsos, G. J., Eds; 1971; Academic Press: New York, Vol. 3, p 139.

as⁵⁶ $K = (\delta_{\text{syn}} - \delta_{\text{obs}})/(\delta_{\text{obs}} - \delta_{\text{anti}})$, where δ_{obs} was the observed chemical shift at different temperatures and δ_{anti} and δ_{syn} were the proton chemical shifts in the anti and syn conformations of **3**, respectively. Note that $\delta_{\text{anti}} = 3.4 \pm 0.1$ and $\delta_{\text{syn}} = 4.2 \pm 0.2$ ppm, as estimated by the linear plot of $1/T$ vs $\ln K$. From the plot of $1/T$ vs $\ln K$ with $R^2 > 0.998$ (as shown in Figure S4 in the Supporting Information), the enthalpy change of the anti/syn transformation was estimated to be 1.5 ± 0.5 kcal/mol, which was consistent with the theoretical calculations. In addition, the fact that the averaged values of methylene (proton) shifts were observed at all temperatures indicated the fast anti/syn transformation on the NMR time scale of 10^{-3} s, even at -80 °C, in agreement with the electrochemical results of **3** (vide infra).

Electrochemistry. Cyclic voltammetry (CV) and Osteryoung square wave voltammetry (OSWV) were performed on a BAS 100A electrochemical analyzer, as described previously.⁹ The electrochemical study of the ortho-bridged donor **3** included a variation of the scan rate from 10 to 2500 mV/s and of the temperature from -30 to $+60$ °C. This revealed that the characteristics of the first oxidation wave ($E_{\text{ox}} = 1.07$ V) did not depend on the temperature and scan rate. The second oxidation wave was temperature and scan-rate dependent. Thus, at room temperature and high scan rate ($1-2$ V s^{-1}) only a single one-electron wave at 1.23 V was observed. However, the decrease of the scan rate resulted in the current decrease of this wave and the appearance and intensity increase of an additional wave at 1.35 V. The ratio of the intensity (or current) of the wave at 1.23 V to that at 1.37 V diminished with decrease of the scan rate and with increasing temperature: i.e., the anodic current at 1.37 V was maximum at low scan rates of 20–50 mV/s and at high temperatures of 50–60 °C, and (vice versa) it was almost absent at high scan rates and/or very low temperatures approaching -30 °C. The first oxidation wave corresponded to the oxidation of the neutral donor to its cation radical, and its potential was determined by the free-energy difference between these two states. In particular, the negative shift of the oxidation potential relative to the mononuclear model and meta and para derivatives **4** and **5** was related to the resonance stabilization in the syn conformation of **3**⁺ (see text). Thus, the scan rate and temperature constancy of the first wave indicated that (a) practically all of the cation radical existed in solution in the syn conformation and (b) there was the possibility of fast interconversion from anti to syn conformations. Indeed, only the syn conformation of **3**⁺ was resonance stabilized. Therefore, if there were a substantial fraction of the anti conformation of **3**⁺ in solution, the syn/anti equilibrium would have been temperature dependent, thus leading to the temperature dependence of the oxidation potential. In addition, the neutral donor **3** existed mainly in the anti conformation and most of cation radical **3**⁺ in the syn conformation. However, the potential of the first oxidation wave was scan-rate independent, which indicated that the anti/syn transformation was fast on the CV time scale; otherwise, a shift of the first oxidation wave to higher potential or even its splitting with an increase in the scan rate would have been observed. The second wave in the cyclic voltammogram of **3** corresponded to the oxidation of the cation radical **3**⁺ to the dication **3**²⁺. The splitting of this wave into two components at slow scan rate and high temperature indicated the existence of an additional transformation affecting this process. Note that the relative (current) intensity of the second positive-shifted component increased with increasing temperature and decreasing scan rate. However, the precise conformational nature of this process is unclear at this juncture.

Isolation of Mixed-Valence Cation-Radical and Dication Salts. The addition of 1 equiv of $\text{NO}^+\text{SbCl}_6^-$ to the mixed-valence donor **3** (4 mM) in dichloromethane at -40 °C produced yellow solutions of the cation radical. After removal of NO (gas) and approximately 50% of the dichloromethane (in vacuo), toluene was added and the dark yellow precipitate of the cation radical was filtered and washed with cold toluene. A similar procedure but with a 1:2 molar ratio of oxidant to donor in order to prevent the disproportionation of the cation radical led to the mixed-valence cation radicals **4**⁺ and **5**⁺. Mixed-valence

dications **4**²⁺ and **5**²⁺ were similarly produced using a 2:1 molar ratio of nitrosonium to the bridged donor. The purities of all salts were determined by iodometric titration and were found to be greater than 98%.¹³ The dication **3**²⁺ and cation radicals and dications of donors **7**–**10** were not isolated in the solid state, owing to partial decomposition in the process of oxidation/isolation; they were therefore prepared and examined in situ, as described below.

UV–Vis–Near-IR Spectroscopic Characterization of the Mixed-Valence Cation Radicals and Dications. The pure isolated salts of the mixed-valence cation radicals and dications were dissolved in dichloromethane, and the UV–vis–near-IR absorption spectra were recorded with a Cary 500 spectrometer. Alternatively, cation radicals and dications were prepared in situ by oxidation with $\text{MG}^+\text{SbCl}_6^-$ with $E_{\text{red}}^{\text{ox}} = 1.55$ V vs SCE. For example, a 1 cm quartz cuvette equipped with a Schlenk adaptor was charged with a freshly prepared stock solution of $\text{MG}^+\text{SbCl}_6^-$ in anhydrous dichloromethane, and a neutral donor such as **3** was added incrementally under an argon atmosphere at -60 °C. The solution immediately took on a yellow coloration, and the UV–vis–near-IR absorption spectrum was recorded. In case of mixed-valence donors **4**, **5**, and **7**, the measurements were taken in the presence of a large excess of neutral donor to ensure the maximum shift of the comproportionation equilibria to the cation radical.⁵⁷

Diffuse-Reflectance Spectroscopy. The single crystals of cation-radical salts with hexachloroantimonate were mixed with potassium hexafluorophosphate (KPF_6), ground to a fine powder to form a 20 wt % dispersion, and stored in a 1 mm quartz cuvette. The diffuse-reflectance spectra were collected on a Cary 500 spectrometer. The spectra were presented as percentage absorption (% ABS) as defined by $\% \text{ABS} = 100(1 - R/R_0)$ with R and R_0 representing the intensities of the diffuse-reflected probe light and of the reference light, respectively.

ESR measurements were performed on either a Bruker ESR-300 X-band or Varian E-line Century 100 ESR spectrometer from $+20$ to -90 °C. The samples were prepared under argon by dissolving the isolated salt in anhydrous dichloromethane or by oxidation with $\text{MG}^+\text{SbCl}_6^-$ or NOSbCl_6 in situ at -60 °C in a Schlenk tube. These solutions were then transferred under an argon atmosphere into a quartz 2 mm diameter ESR tube connected to a 5 mL Pyrex tube equipped with a Teflon valve. The tube was placed in a quartz Dewar placed in the center of a the rectangular cavity, and the temperature was regulated by an IBM temperature controller to within ± 0.5 K. Compressed nitrogen was guided through the cavity to remove any adventitious moisture condensed onto the Dewar surface at low temperatures. ESR simulations were carried out with the PEST WinSim program, version 0.96 (Public EPR Software Tools, National Institute of Environmental Health Sciences), by variation of the splitting parameters and line widths to obtain the best correspondence of simulated and experimental spectra. The ESR hyperfine splittings of the mononuclear model **6**⁺ were used as the starting set of parameters.²⁶ Dynamic ESR spectra simulations were carried out with the aid of the ESR-EXN program.³¹ In these cases, the parameters obtained in the ESR simulation for the mononuclear model cation radical were used as the starting point, and the rate constants were varied to obtain the best correspondence between the calculated and experimental spectra. The electron-transfer rate constants k_{ET} evaluated from the line-broadening experiments were most reliable in a rather narrow (temporal) range: $5 \times 10^6 < k_{\text{ET}} < 10^8$ s^{-1} . At slower rates, the line broadening was insufficient to be observed; at faster rates the line broadening was too severe. When the ET rate constant was very high on the ESR time scale of $\tau < 10^{-9}$ s, the values of the hyperfine splittings became nearly half and the number of nuclei doubled as compared with those at the slow-rate limit. We were unable to carry out precise dynamic ESR spectral simulations in the fast-

(57) The electronic and ESR spectra were essentially unaffected when the molar ratio of the neutral donor to cation radical was deliberately varied from 2:1 to 10:1, indicating that the effects of comproportionation can be neglected.

exchange limit. To exclude effects of methoxyl group rotation, the temperature dependence of the ESR spectrum of $7^{+\bullet}$ was measured at relatively low temperatures (-80 to -30 °C).^{57,58} Likewise, to exclude any contribution of the comproportionation equilibria on the line broadening of $7^{+\bullet}$, the ESR spectra were measured in the presence of added donor **7**—and found to be invariant with various amounts in excess. Owing to the limited (insufficiently resolved) experimental data, computer simulations of the ESR spectra of cation radicals $9^{+\bullet}$ and $10^{+\bullet}$ can also be derived from alternative sets of splitting parameters (e.g. $a_{\text{OCH}_3} = 3.2$ G, $a_{\text{CH}} = 6.9$ and 1.7 G, and $a_{\text{ArH}} = 0.5$ G). As such, the data presented for these entries in Table 3 are considered tentative and subject to further verification.

X-ray Crystallography of the Cation Radicals. The intensity data were collected with aid of a Siemens SMART Apex diffractometer equipped with a CCD detector using Mo K α radiation ($\lambda = 0.71073$ Å), at -150 °C unless otherwise specified. The structures were solved by direct methods and refined by full-matrix least-squares procedures with IBM Pentium and SGI O₂ computers.⁵⁹ Note that the X-ray structure details of various compounds mentioned here are on deposit and can be obtained from the Cambridge Crystallographic Data Center, 12 Union Road, Cambridge CB2 1EZ, U.K. A yellow solution of (2 mM) nitrosonium hexachloroantimonate ($\text{NO}^+\text{SbCl}_6^-$) and **3** (2 mM) in dichloromethane (20 mL) was prepared under an argon atmosphere at -60 °C. The solution was carefully layered with toluene and placed in the cold bath (-60 °C). After 7 days, dark green single crystals were formed as the cation-radical salt ($3^{+\bullet}\text{SbCl}_6^-$) suitable for X-ray crystallographic analysis. Single crystals of the cation-radical salt $3^{+\bullet}\text{PF}_6^-$ were similarly obtained using tris(4-bromophenyl)amine cation radical hexafluorophosphate as the oxidant. Single crystals of the neutral

Table 8. Crystallographic Data for Aromatic Donors and Their Cation Radicals

	$3 \cdot 0.75\text{CH}_2\text{Cl}_2$	$3^{+\bullet}\text{SbCl}_6 \cdot \text{CH}_2\text{Cl}_2$	$3^{+\bullet}\text{PF}_6 \cdot \text{CH}_2\text{Cl}_2$
empirical formula	$\text{C}_{30.75}\text{H}_{39.5}\text{Cl}_{1.5}\text{O}_4$	$\text{C}_{31}\text{H}_{40}\text{Cl}_8\text{O}_4\text{Sb}$	$\text{C}_{31}\text{H}_{40}\text{Cl}_2\text{F}_6\text{O}_4\text{P}$
formula wt	526.30	881.98	692.50
cryst syst	triclinic	triclinic	monoclinic
space group	$P\bar{1}$	$P\bar{1}$	$P2_1/c$
a , Å	8.445(1)	10.126.1(1)	11.348(1)
b , Å	12.666(2)	13.043(1)	10.152(1)
c , Å	13.717(2)	14.533(1)	27.762(2)
α , deg	94.64(1)	77.25(1)	90
β , deg	91.18(1)	84.41(1)	93.23(1)
γ , deg	99.10(1)	81.52(1)	90
V , Å ³ /Z	1443.1(3)/2	1847.4(2)/2	3193.3(5)/4
ρ_{calcd} , g/cm ³	1.211	1.586	1.440
total/unique	20 598/12 410	18 985/10 746	26 315/10 459
no. of rflns			
no. of data ($I > 2\sigma(I)$)	7795	7815	7806
$R1^a/wR2^b$	0.059/0.163	0.042/0.089	0.057/0.154

$$^a R1 = \sum ||F_o| - |F_c|| / \sum |F_o|. \quad ^b wR2 = \{ \sum [w(F_o^2 - F_c^2)^2] / \sum [w(F_o^2)^2] \}^{1/2}.$$

mixed-valence donor **3** were obtained by slow evaporation of the solvent. Crystallographic data for the pertinent aromatic donors and their cation radicals are presented in Table 8.

Acknowledgment. We thank Professor S. F. Nelsen for kindly providing us with a copy of the ESR-EXN line-broadening program, J. M. Lu for help with the ESR spectral measurements, and the R. A. Welch Foundation and National Science Foundation for financial support.

Supporting Information Available: Temperature dependence of the chemical shifts in the ¹H NMR spectrum of **3** (Table S1), ESR spectra of dications 3^{2+} , 4^{2+} , and 5^{2+} (Figure S1), solid-state (UV–vis–near-IR) spectra of cation radicals $3^{+\bullet}$, $4^{+\bullet}$, and $6^{+\bullet}$ as the SbCl_6^- salts (Figure S2), temperature dependence of the syn/anti equilibrium constant in the mixed-valence donor **3** (Figure S3), and Arrhenius activation energy for intramolecular electron exchange (k_{ET}) in the sterically hindered mixed-valence cation radical $7^{+\bullet}$ (Figure S4). This material is available free of charge via the Internet at <http://pubs.acs.org>.

JA037867S

- (58) Temperature dependence of the hyperfine splitting constants due to the rotation of the methoxyl group was described by Sullivan in ref 27. Since such an effect was most pronounced in cation radicals containing a methoxyl and (additionally) two ortho-substituted groups,²⁷ it did not substantially affect the temperature dependence of the ESR spectra of cation radicals $2^{+\bullet}$ – $6^{+\bullet}$. However, methoxyl rotation in $7^{+\bullet}$ can account for noticeable changes in the hyperfine splitting constants and the appearance of additional components in ESR spectra at room temperature similar to those observed in the ESR spectrum of the cation radical of the mononuclear sterically hindered donor 9,10-dimethoxy-1,4:5,8-dimethano-1,2,3,4,5,6,7,8-octahydroanthracene ($\text{CRET}^{+\bullet}$).^{30c} However, for $\text{CRET}^{+\bullet}$, the ESR spectra were invariant in the temperature range from -90 to -20 °C, and the line widths were practically constant at all temperatures. The same temperature-independent ESR spectra were observed in the -90 to -20 °C range for the mononuclear model $8^{+\bullet}$. We thus conclude that line broadening observed in the ortho-bridged cation radical $7^{+\bullet}$ in the temperature range -90 to -30 °C can be reliably assigned to intramolecular electron transfer.
- (59) Sheldrick, G. M. SHELXS-86, Program for Structure Solution; University of Göttingen, Göttingen, Germany, 1986.